The Energy Budget of the NCAR Community Climate Model: CCM3*

J. T. KIEHL, J. J. HACK, AND J. W. HURRELL

National Center for Atmospheric Research,[+] *Boulder, Colorado*

(Manuscript received 30 April 1997, in final form 17 October 1997)

ABSTRACT

The energy budget of the latest version of the National Center for Atmospheric Research (NCAR) Community Climate Model (CCM3) is described. The energy budget at the top of the atmosphere and at the earth's surface is compared to observational estimates. The annual mean, seasonal mean, and seasonal cycle of the energy budget are evaluated in comparison with earth radiation budget data at the top of the atmosphere and with the NCAR Ocean Model (NCOM) forcing data at the ocean's surface. Individual terms in the energy budget are discussed. The transient response of the top-of-atmosphere radiative budget to anomalies in tropical sea surface temperature is also presented. In general, the CCM3 is in excellent agreement with ERBE data in terms of annual and seasonal means. The seasonal cycle of the top-of-atmosphere radiation budget is also in good ($<$10 W m^{-2}) agreement with ERBE data. At the surface, the model shortwave flux over the oceans is too large compared to data obtained by W. G. Large and colleagues ($\sim$20–30 W m^{-2}). It is argued that this bias is related to a model underestimate of shortwave cloud absorption. The major biases in the model are related to the position of deep convection in the tropical Pacific, summertime convective activity over land regions, and the model's inability to realistically represent marine stratus and stratocumulus clouds. Despite these deficiencies, the model's implied ocean heat transport is in very good agreement with the explicit ocean heat transport of the NCOM uncoupled simulations. This result is a major reason for the success of the NCAR Climate System Model.

1. Introduction

The flow of energy through the climate system is a fundamental property that climate system models and their components should simulate well. The net flux of energy at the top of the atmosphere determines the available energy for the complete climate system (i.e., atmosphere and underlying surfaces). However, an equally important property is the transformation of this radiative energy into other forms—such as kinetic, latent, and sensible—with the vertical and horizontal redistribution of these forms of energy. The present work describes the simulated energy budget of the latest atmospheric global climate model at the National Center for Atmospheric Research (NCAR), the Community Climate Model (CCM3). Previous studies have discussed the earth radiation budget for earlier versions of the CCM [e.g., Kiehl and Ramanathan (1990) for CCM1 and Kiehl et al. (1994) for CCM2]. The present study not only describes the radiation budget of CCM3 but carries out a more extensive analysis of the entire energy budget of the atmospheric model at both the top of the atmosphere and the surface. There is added emphasis on the surface energy budget, since the CCM3 is the atmospheric component of the NCAR Climate System Model (CSM) (see Boville and Gent 1998; Boville and Hurrell 1998). The accuracy of the surface fluxes is important for the land, ocean, and sea-ice components of the CSM.

To objectively evaluate the accuracy of both the top-of-atmosphere and surface energy budgets, precise observations are required (see Kiehl and Trenberth 1997). At the top of the atmosphere, the Earth Radiation Budget Experiment (ERBE) provides calibrated and accurate data to assess the CCM3 simulation. At the surface, there are larger uncertainties in the magnitude and spatial distribution of energy fluxes. Various global grided datasets exist for model evaluation (e.g., Oberhuber 1988; Bishop and Rossow 1991). However, it is widely recognized (Gleckler and Weare 1995) that these datasets are uncertain to 30 W m^{-2}. Over the oceans the largest uncertainties are in the net solar flux and the latent heat flux. Over sea ice there can be large uncertainties in both the estimated net shortwave and longwave fluxes. A discussion of the energy budget over land surfaces is presented in Bonan (1998). The focus of this study will be on the surface energy budget over

* An electronic supplement to this article may be found on the CD-ROM accompanying this issue or at http://www.ametsoc.org/AMS.

[+] The National Center for Atmospheric Research is sponsored by the National Science Foundation.

Corresponding author address: Dr. Jeffrey T. Kiehl, NCAR/CGD, P.O. Box 3000, Boulder, CO 80307-3000.
E-mail: jtkon@ucar.edu

oceans. We employ the recent NCAR Ocean Model (NCOM) forcing data for model evaluation purposes (Large et al. 1997).

The study is organized as follows: section 2 provides a brief description of CCM3, section 3 describes the global and zonal-mean energy budget from the model and makes comparisons to observations, section 4 considers the geographic distribution of the annual mean energy terms, section 5 provides a regional and seasonal analysis of the budget, section 6 considers the response of the energy budget to anomalies in tropical sea surface temperatures, and finally section 7 summarizes the findings in the study.

2. Model description

A detailed description of all the physical and numerical methods used in CCM3 are provided in Kiehl et al. (1996). A summary of the changes in the physics and numerics employed in CCM3 compared to those used in CCM2 are given in Kiehl et al. (1998). Kiehl et al. (1998) also summarize key differences in the model simulation between CCM3 and CCM2. The NCAR CCM3 is a global spectral climate model. The standard resolution of the model is T42 (equivalent to 2.8° lat $\times$ 2.8° long) with 18 layers in the vertical. Shortwave and longwave fluxes are calculated every hour. The model time step is 20 min. Between the hourly radiative calculations, these fluxes are held fixed. The radiative effects of clouds are updated every hour.

A major change between CCM2 and CCM3 is the inclusion of the longwave radiative effects of CH_4, N_2O, CFC11, and CFC12. The CCM3 also includes the longwave properties of two weak CO_2 bands located at 9.4 and 10.4 μm, which are important for certain paleoclimate problems. In the shortwave clear sky, the CCM3 now crudely includes the effects of a background aerosol by using a uniform aerosol with a visible optical depth of 0.14. The radiative properties of the aerosol are identical to sulfate aerosols, and the aerosol is uniformly distributed in the lowest three model layers ($\sim$1000 m in depth). It is recognized that aerosols have large spatial and temporal variability and their optical properties are quite diverse. The current approach accounts, in a crude fashion, for the importance of these aerosols to the shortwave budget. As will be seen, this significantly improves the comparison of the model shortwave clear sky budget with ERBE data. In the future, the model will include more realistic aerosol properties. The longwave effects of the boundary layer aerosol are neglected.

For cloudy skies, there have been significant changes in the cloud radiative properties from CCM2 to CCM3. The CCM3 distinguishes between the radiative properties of liquid, mixed phase, and ice cloud particles. The effective cloud particle size depends on phase and on whether clouds are located over continental or maritime regions. The ice cloud radiative properties are based on the work of Ebert and Curry (1992), and the specification of continental versus maritime particle size follows the work of Kiehl (1994a). The cloud water is diagnosed in terms of local column water vapor (Hack 1997) and is distributed in the vertical according to a liquid water scale height. Thus, CCM3 accounts for local variations in cloud water, unlike CCM2.

The cloud fraction in each layer is diagnosed in terms of relative humidity, static stability, and vertical velocity. Convective cloud fraction is diagnosed in terms of cloud mass flux. Essentially, three cloud types are diagnosed: convective cloud, large-scale stable cloud, and stratus associated with low-level inversions (i.e., marine stratus). Clouds are allowed to form in any model layer, excluding the layer nearest the surface. The cloud fraction is assumed to be randomly overlapped in the vertical. In the shortwave this overlap is accounted for by weighting the cloud optical depth by the cloud fraction to the three-halves power (Briegleb 1992). In the longwave spectral region, the total flux is a linear function of the overcast and clear sky fluxes within each grid box.

For the nonradiative flux terms, the major changes affecting the CCM3 energy budget are the following: improvements in the boundary formulation, a new parameterization for deep convection, and changes in the surface roughness over oceans. These changes have made large changes in the latent heat fluxes over oceans (e.g., Collins et al. 1997, hereafter CO97). Details of these changes are given in Kiehl et al. (1998) and Zhang et al. (1998).

The results presented in this study are based on a 15-yr integration using observed monthly mean SSTs from 1979 to 1993. Thus, this simulation is an extension of the 10-yr Atmospheric Model Intercomparison Project type of integration (1979–89). A number of datasets are employed for evaluation of the CCM3 simulation. At the top of the atmosphere, model results are averaged from 1985 to mid-1989 for comparison to the ERBE. At the surface, we employ the Large et al. (1997) surface fluxes. These surface fluxes are based on a number of datasets from satellite retrievals (Bishop and Rossow 1991) and near-surface state information from the recent National Centers for Environmental Prediction (NCEP) reanalysis (Kalnay et al. 1996). Surface fluxes are computed from empirical relations and bulk formula from these data. Parts of the Large et al. data were used to force the uncoupled CSM ocean model in the spinup phase (see Gent et al. 1998). It must be recognized that there are uncertainties in these observationally based surface fluxes. Thus, it is best to view the model comparison with these fluxes as qualitative and not highly quantitative. A description of the dynamical climatology of CCM3 is provided in Hurrell et al. (1998), and the hydrologic cycle of CCM3 is presented in Hack et al. (1998). The purpose of the present study is to focus on the energy budget of CCM3.

TABLE 1. Ensemble global annual mean top-of-atmosphere (TOA) and surface energy budgets. Fluxes are in W m^{-2}. Cloud fraction is in percent. OLR denotes outgoing longwave flux in observations, but net longwave flux from CCM3; LWCF is longwave cloud forcing; and SWCF is shortwave cloud forcing. Observational estimates are summarized from Kiehl and Trenberth (1997).

Field	Observation	CCM3
	Top of atmosphere	
OLR	234.8	236.97
Clear sky OLR	264.0	266.22
Solar absorbed	238.1	236.88
Clear solar abs.	286.3	286.42
LWCF	29.2	29.25
SWCF	−48.2	−49.54
Net TOA	3.3	−0.09
Cloud fraction	52.2–62.5	58.83
	Surface fluxes	
Solar absorbed	142–168	171.05
Clear solar abs.	217.2*	220.83
Net longwave	45.8*–66	60.68
Clear net LW	70.7*	92.39
Latent heat	78	89.97
Sensible heat	24	20.47
Net surface	0.00	−0.07

* Rossow and Zhang (1995).

TABLE 2. Ensemble global annual-mean surface energy budget. Fluxes are in W m^{-2}. Observational estimates are summarized from Large et al. (1998), and shortwave flux in parentheses is from Bishop and Rossow (1991).

Field	Observation	CCM3
	Surface fluxes	
Solar absorbed	164.4 (188)	191.1
Net longwave	53.6	59.6
Latent heat	100.6	114.8
Sensible heat	9.1	16.2

3. Global and zonal-mean budgets

Table 1 presents the globally averaged ensemble annual mean energy budget for CCM3 and various observations. The global top-of-atmosphere model fluxes were tuned to agree with the ERBE fluxes to within a few W m^{-2}. The balance was accomplished by tuning the model cloud fraction and global mean aerosol optical depth. The net flux at the top of the atmosphere is −0.09 watts per square meter. This order of balance is required, since the model is the atmospheric component of the CSM (Boville and Gent 1998). To prevent initial drift in the coupled system, the net top-of-atmosphere flux must be small (i.e., less than a few tenths of a W m^{-2}). At the surface, we compare the model flux with the estimates of Kiehl and Trenberth (1997), who note there is substantial uncertainty in the shortwave surface flux (around 25 W m^{-2}). For example, Ohmura and Gilgen (1993), using surface observations, estimate a much smaller net surface shortwave flux (142 W m^{-2}). There are also large uncertainties in global annual mean latent heat flux.

Energy conservation imposes the constraint that the sum of the surface fluxes must be zero. Thus, any changes to a particular flux component (e.g., the net shortwave flux) will require changes in the other flux terms (e.g., latent and sensible heat). These types of changes between surface shortwave flux and latent heat flux occurred in developing CCM3 from CCM2. The 15-yr ensemble-mean net surface fluxes from CCM3 sum to −0.07 W m^{-2}, which results from the near-zero top-of-atmosphere net balance (which was tuned) and the high order of energy conservation within the model atmosphere.

The agreement between the observed and modeled clear sky top-of-atmosphere longwave flux is a result of the addition of the various trace gases to CCM3. The bias in this field for CCM2 was 7 W m^{-2}. The importance of various trace gases and ''weak bands'' of carbon dioxide and ozone to the top-of-atmosphere (TOA) clear sky outgoing longwave was pointed out by Kiehl and Briegleb (1992). In the shortwave, the addition of a tropospheric aerosol with visible optical depth of 0.14 has significantly improved the clear sky top-of-atmosphere model value. Note that a global aerosol optical depth of 0.14 is close to the observational estimate of Andreae (1995) of 0.149. Over ocean regions the visible aerosol optical depth is slightly smaller; that is, ~0.12 (e.g., Villevalde et al. 1994; Porter and Clarke 1994). The bias in the TOA shortwave clear sky flux in CCM2 was 9 W m^{-2}. In CCM3 the agreement with the ERBE TOA data is ~2 W m^{-2}. At the surface the clear sky absorbed shortwave flux from the model agrees to within 2 W m^{-2} with the Rossow and Zhang (1995) estimate. Thus, globally there is good agreement in the clear sky shortwave flux. Regionally, the bias in clear sky shortwave flux will depend on an accurate description of the aerosol properties for that region.

At the surface, the model latent heat flux is at the upper bound of observational estimates (78–90 W m^{-2}). The net shortwave flux is in good agreement with the model-derived value of Kiehl and Trenberth (1997), but the range of observational estimates is quite large (142–165 W m^{-2}). Hence, the CCM3 value could be in error by a substantial amount. Indeed, comparison with Global Energy Balance Archive station data indicate that CCM3 surface shortwave fluxes are too large (Zhang et al. 1998). As stated above, if the model surface shortwave flux were to be reduced to 142 W m^{-2}, a reduction would also be required in the other surface flux terms, most likely the latent heat flux (see Kiehl et al. 1995), which would bring the CCM3 latent heat flux in closer agreement with the midrange of the observational estimates. A similar difference in shortwave flux occurs over ocean regions. Table 2 shows the global annual mean surface energy budget for ocean regions. The difference between the shortwave flux from CCM3 and

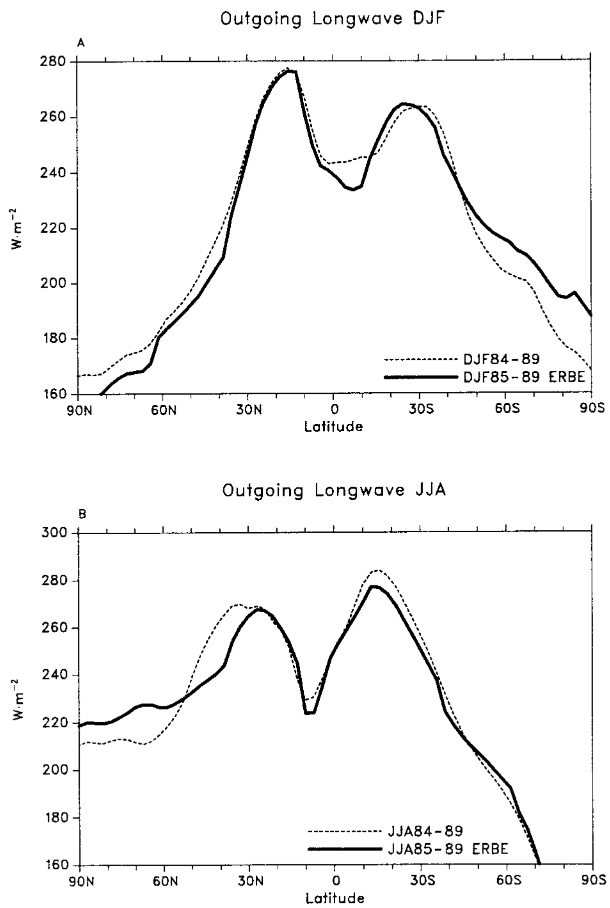

FIG. 1. Ensemble-mean zonally averaged outgoing longwave radiative flux (W m^{-2}) for (a) DJF and (b) JJA seasons for the CCM3 (-----) and the ERBE data (———). Averaging period is from 1984 to 1989.

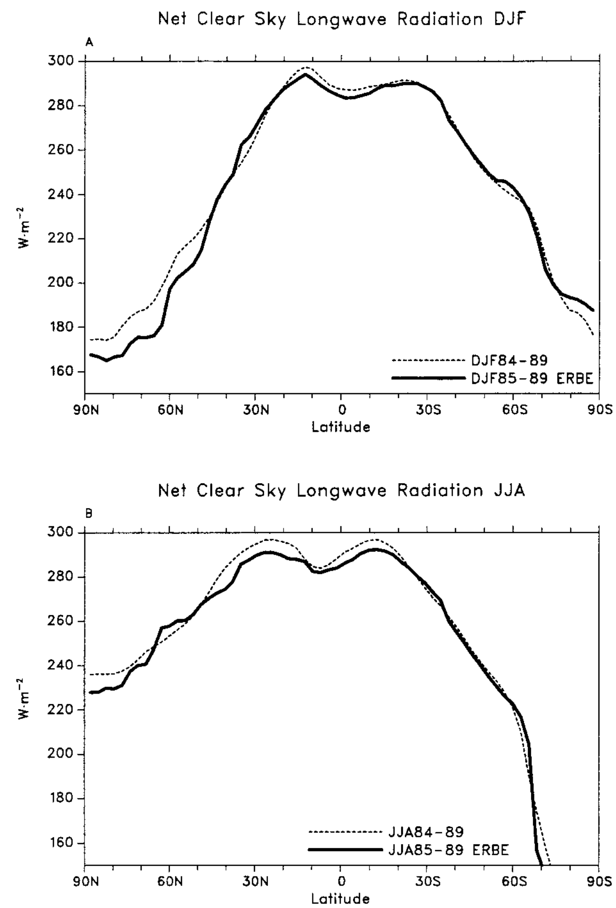

FIG. 2. Ensemble-mean zonally averaged clear sky outgoing longwave radiative flux (W m^{-2}) for (a) DJF and (b) JJA seasons for the CCM3 (-----) and the ERBE data (———). Averaging period is from 1984 to 1989.

that of Large et al. (1997) is 30.6 W m^{-2}. The CCM3 shortwave flux is in better agreement with the Bishop and Rossow (1991) results ($\sim$7 W m^{-2}). The model latent heat flux is $\sim$17 W m^{-2} larger than the estimate by Large et al.

The zonally averaged outgoing longwave flux for the ensemble averages of December–February (DJF) and June–August (JJA) from 1984 to 1989 from the CCM3 and the ERBE data show good agreement (i.e., less than 10 W m^{-2}) for both seasons (Fig. 1). The largest biases exist at high latitudes for local hemispheric summer conditions, where the model underestimates the OLR compared to ERBE. The zonally averaged clear sky outgoing longwave flux, however, is in good agreement in these regions (Fig. 2). Thus, the bias in the outgoing longwave flux must be due to cloud properties and not temperature and/or moisture biases, since these would appear in the clear sky outgoing longwave flux. The good agreement in the clear sky top-of-atmosphere flux is due, in large part, to the incorporation of the radiative effects of CH_4, N_2O, and CFCs.

In the shortwave spectral region, the zonally averaged planetary albedo for DJF and JJA is shown in Fig. 3. There is very good agreement between the model and observations in DJF, while in JJA the model is too bright at high latitude summer in both hemispheres, with the largest bias existing in Northern Hemisphere summer between 60° and 80°. This bias supports the conclusion that the bias in outgoing longwave radiation (OLR) is due to excessive cloud cover and/or an overestimation in cloud optical thickness. Comparison of the CCM3 cloud cover and cloud liquid water path with observations (Hack et al. 1998) supports this conclusion. There is also a small bias in the subtropics, where the model overestimates the planetary albedo. Note that these biases cannot be attributed to surface albedo, since the clear sky albedo in these regions is in excellent agreement with ERBE (Fig. 4). There is an underestimate in clear sky albedo in NH winter poleward of 50°. This is no doubt associated with an underprediction of snow cover and/or snow reflective properties.

Retrieval of clear sky radiative properties poleward of 70 is complicated by the presence of highly reflective surfaces (i.e., snow or ice); thus we restrict comparison

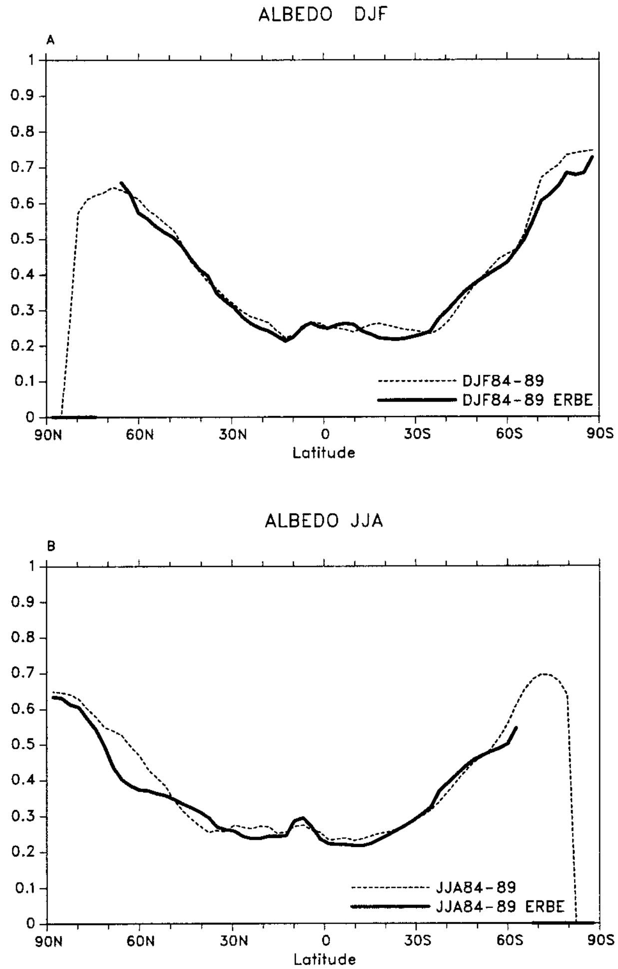

FIG. 3. Ensemble-mean zonally averaged planetary albedo for (a) DJF and (b) JJA seasons for the CCM3 (-----) and the ERBE data (———). Averaging period is from 1984 to 1989.

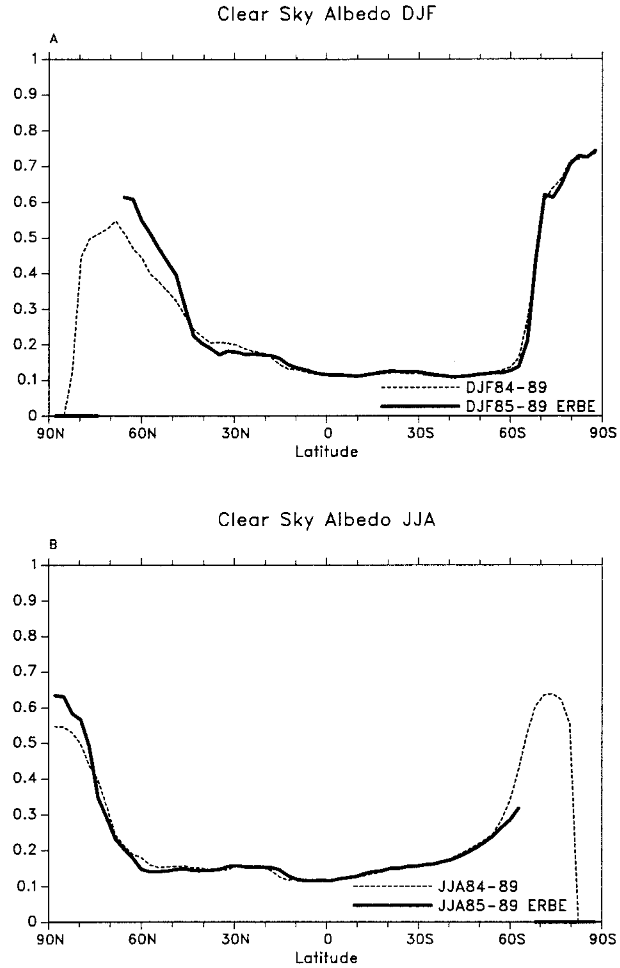

FIG. 4. Ensemble-mean zonally averaged clear sky planetary albedo for (a) DJF and (b) JJA seasons for the CCM3 (-----) and the ERBE data (———). Averaging period is from 1984 to 1989.

of the cloud radiative forcing to 70° north and south. The zonal mean of longwave cloud radiative forcing (LWCF) is shown in Fig. 5. LWCF is defined as the difference between the clear sky and all sky outgoing longwave radiative flux. This property is a quantitative measure of the greenhouse trapping effect of clouds (see, e.g., Kiehl and Trenberth 1997). There are three maxima in the zonal mean that are associated with extratropical storm track cloud systems and tropical convective cloud systems. The model represents the tropical maxima in LWCF very well for both seasons. In the extratropics, the model LWCF in the summer hemisphere is too far poleward and north of 50° is too large. This is another indication that the cloud fraction and/or cloud emissivity is too large in the CCM3 for extratropical summertime cloud systems. Note that the bias in NH summer is actually due more to a poleward shift, by about 10° in latitude, of the model cloud forcing.

In the shortwave, the cloud forcing (SWCF) is defined as a difference between all sky and clear sky shortwave absorbed flux. Figure 6 shows the zonally and seasonally averaged SWCF from CCM3 and from ERBE. A significant bias existed in the CCM2 SWCF [see Fig. 10 of Kiehl et al. (1994)], where the model underpredicted the zonal-mean local summertime values. This underprediction had serious implications for the model-calculated implied ocean heat transport (Gleckler et al. 1995). The CCM3, however, does capture the local minimum in SWCF due to the extratropical storm tracks. There is now an overestimate of this forcing in NH summer poleward of 50°. The bias in subtropical clouds is apparent in the SWCF, where the model forcing is too large by as much 20 W m^{-2} at some latitudes. This is now the largest bias in the SWCF in CCM3.

At the surface, we consider each term in the energy budget separately, and then the net surface energy budget. We restrict our comparison to ocean regions and to long-term annual mean conditions to minimize the storage term in the energy budget. The surface energy budget over land is discussed in the study by Bonan (1998).

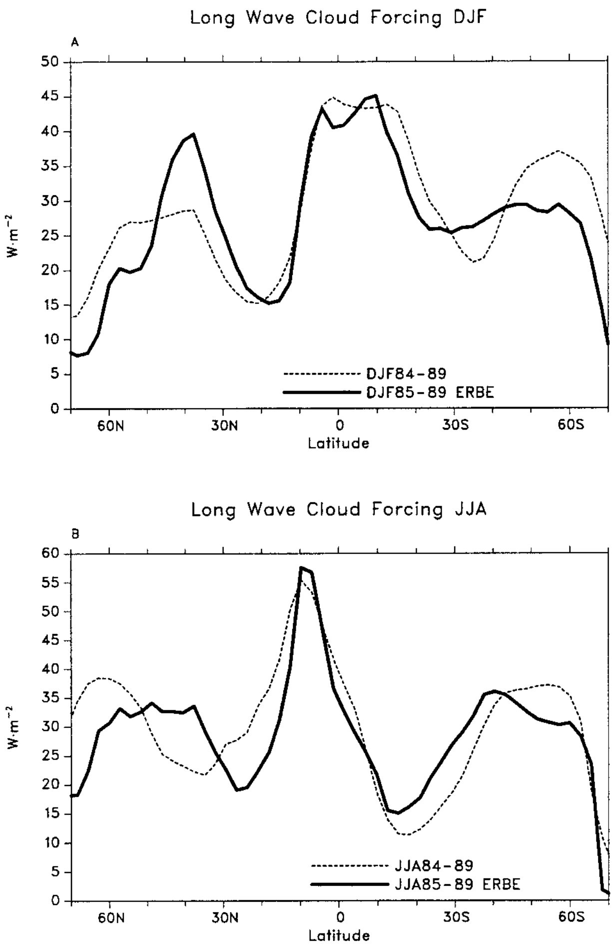

FIG. 5. Ensemble-mean zonally averaged longwave cloud forcing (W m^{-2}) for (a) DJF and (b) JJA seasons for the CCM3 (-----) and the ERBE data (———). Averaging period is from 1984 to 1989.

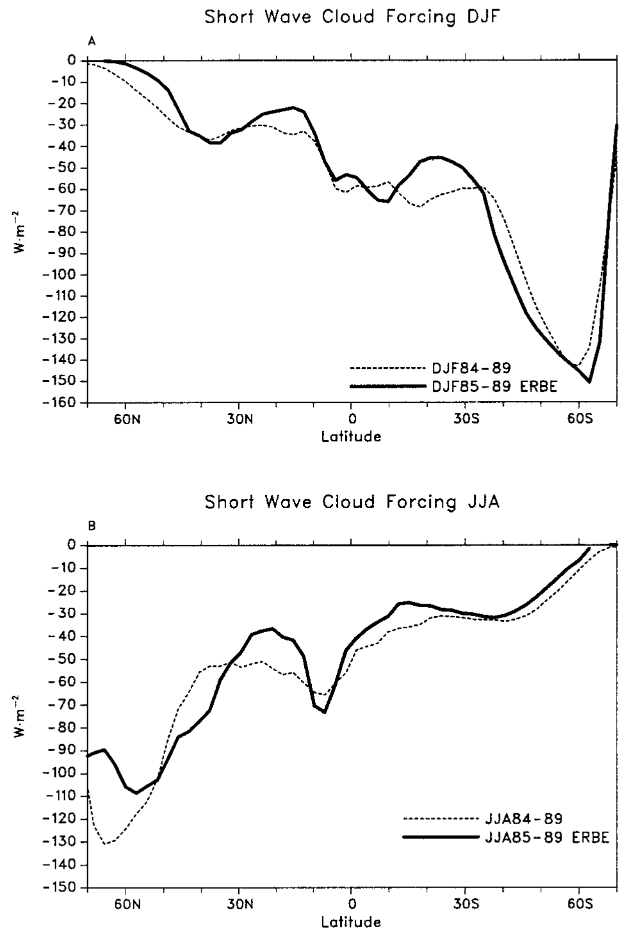

FIG. 6. Ensemble-mean zonally averaged shortwave cloud forcing (W m^{-2}) for (a) DJF and (b) JJA seasons for the CCM3 (-----) and the ERBE data (———). Averaging period is from 1984 to 1989.

Figure 7 shows the net annual and zonal-mean shortwave flux over oceans. There is a significant bias in the model surface shortwave flux compared to the Large et al. forcing data. Note that if we were to compare the model fluxes with the results of Bishop and Rossow (1991) the two fields would agree fairly well. Large et al. (1997) reduced the values of Bishop and Rossow by 12.5% to bring the satellite retrieved results closer to ship observations. The adjusted shortwave fluxes also produce a much more realistic distribution of SSTs in the uncoupled ocean model (see Gent et al. 1998). In the Tropics the difference between the Large et al. data and the CCM3 is ~30 W m^{-2}, which is close to the 35 W m^{-2} bias discussed by Ramanathan et al. (1995) for the warm pool region. The other large surface energy term for the oceans is the latent heat flux (Fig. 8). At most latitudes the agreement is quite good, given the differences in data sources used to obtain the observational estimate. In the Southern Hemisphere, CCM3 tends to overpredict the latent heat flux by 10–20 W m^{-2}, while in the Northern Hemisphere the model un-

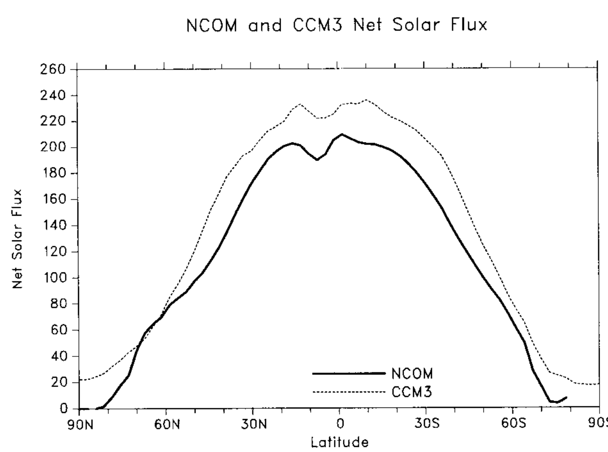

FIG. 7. Ensemble-mean annual and zonal mean over oceans of the net shortwave flux (W m^{-2}) at the surface for CCM3 (-----) and the observationally based Large et al. data (———).

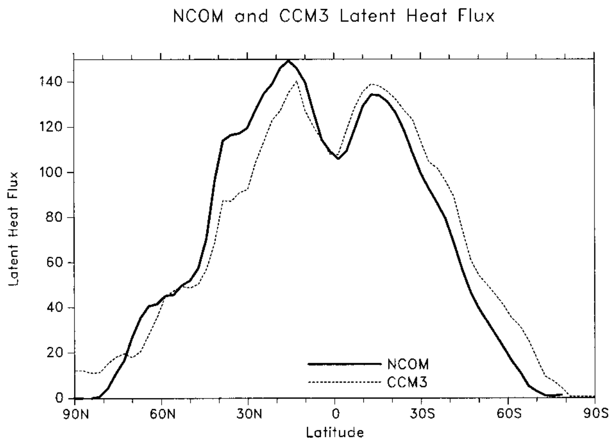

FIG. 8. Ensemble-mean annual and zonal mean over oceans of the latent heat flux (W m^{-2}) at the surface for CCM3 (-----) and the observationally based Large et al. data (———).

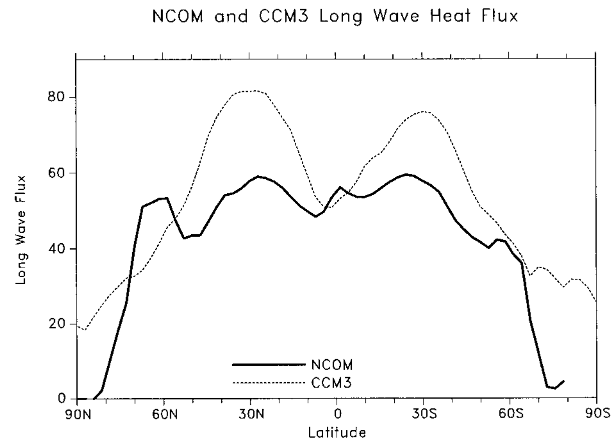

FIG. 9. Ensemble-mean annual and zonal mean over oceans of the net longwave flux (W m^{-2}) at the surface for CCM3 (-----) and the observationally based Large et al. data (———).

derpredicts the latent heat flux by a similar amount. The equatorial minimum in flux is captured quite well in CCM3 (see also CO97).

A smaller term in the ocean surface energy flux is the net longwave flux, which depends critically upon cloud-base height, cloud fraction, and lower-tropospheric moisture. The lack of observational data on these quantities (especially over the oceans) means that the Large et al. data are more uncertain. Figure 9 shows the annual and zonal mean of the net surface longwave flux from the CCM3 and the Large et al. data. These results indicate that the model's downward longwave flux is perhaps too low in the subtropical oceans, yielding an overestimate in the net flux (i.e., upward minus downward). The net longwave flux from Large et al. is determined by an empirical relationship that depends on sea surface and surface air temperatures, specific humidities, and total cloud fraction (Large et al. 1997). There is no explicit dependence on cloud base height. Large et al. (1997) use the total cloud cover from the International Satellite Cloud Climatology Project (ISCCP) climatology (Rossow and Schiffer 1991). Comparison of the total cloud cover from ISCCP and the CCM3 (Fig. 10) indicates that ISCCP generally has higher total cloud cover. In the subtropics, the ISCCP cloud cover is larger than in the CCM3, and this is one source of the bias in longwave flux. It is interesting to note that the *Nimbus-7* cloud cover (see Fig. 10) is significantly lower ($\sim$10%) than ISCCP in the subtropical regions (Mokhov and Schlesinger 1994). Thus, if Large et al. had employed *Nimbus-7* total cloud cover, the agreement in longwave flux between Large et al. and the CCM3 would be much better in these regions. Another possible source of the bias is related to the CCM longwave radiation model. An underestimate in the downward flux for low humidity conditions above the atmospheric boundary layer has been noted in column radiation calculations with the CCM model. Some of the bias seen in Fig. 9 could be due to this problem in the radiation model. We have traced this problem back to a bias in the asymptotic behavior of the water vapor rotation band.

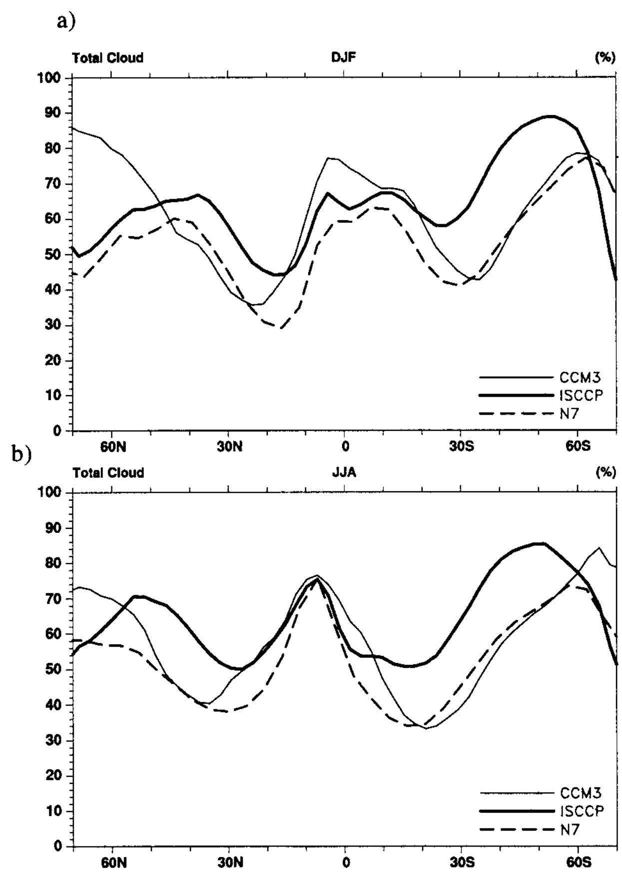

FIG. 10. Ensemble-mean zonally averaged total cloud amount (%) for (a) DJF and (b) JJA seasons for the CCM3 (———) and the ISCCP data (▬▬) and *Nimbus-7* (– – –).

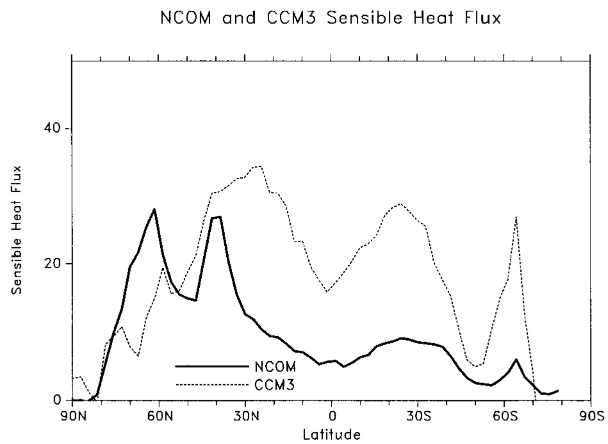

FIG. 11. Ensemble-mean annual and zonal mean over oceans of the sensible heat flux (W m^{-2}) at the surface for CCM3 (-----) and the observationally based Large et al. data (———).

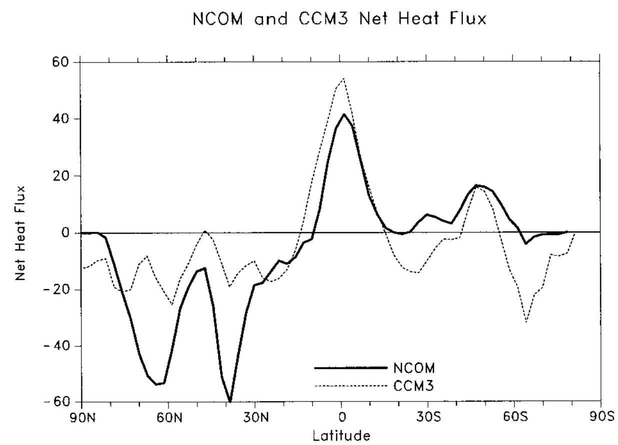

FIG. 12. Ensemble-mean annual and zonal mean over oceans of the total energy flux (W m^{-2}) at the surface for CCM3 (-----) and the observationally based Large et al. data (———).

The smallest surface energy flux term over oceans is due to sensible heat exchange (Fig. 11). The observational estimate of this flux is again very uncertain. In general, the model sensible heat flux is larger than the Large et al. estimate, which is related to differences in surface wind speed between the CCM3 and the NCEP reanalysis (Hurrell et al. 1998).

For the ocean, of course, it is the total flux of energy across the surface that is of greatest importance. This quantity directly determines the ocean heat transport (Gleckler et al. 1995). Differences between a model surface net heat flux and observations will be a source of climate drift. Indeed, past attempts to correct biases in coupled model surface heat fluxes are the source of flux adjustment or flux correction (Kerr 1995). If small biases exist between the model surface flux and observations, then there is little need for flux corrections. Figure 12 shows the annual mean, zonal-mean net (i.e., net shortwave minus latent minus longwave minus sensible heat) surface energy flux from the CCM3 and the Large et al. data. For most latitudes the agreement between these datasets is good. The largest biases exist in the mid- to high latitudes of the Northern Hemisphere.

A fundamental quantity for the climate system is the poleward transport of heat for the entire climate system, and the partitioning of this transport between the atmosphere and the ocean (see Trenberth and Solomon 1994). Since the CCM3 is the atmospheric component of the fully coupled NCAR CSM (Boville and Gent 1998), it is important to consider the implied ocean heat transport in the CCM3 (see Gleckler et al. 1995). The ''implied'' ocean heat transport from the atmospheric model is what the ocean must transport given prescribed SSTs. One can obtain the implied heat flux by either subtracting the atmospheric heat transport from the total heat transport derived from the top-of-atmosphere net radiative imbalance, or directly from the net surface flux. These quantities will be identical, to the degree that the atmospheric model conserves energy. Results shown in Table 1 indicate that the CCM3 atmospheric model conserves energy to a high degree of accuracy.

Figure 13 shows the zonal- and annual-mean absorbed shortwave flux, outgoing longwave flux, and net radiative flux (shortwave minus longwave) from CCM3 and from ERBE. There is excellent agreement between

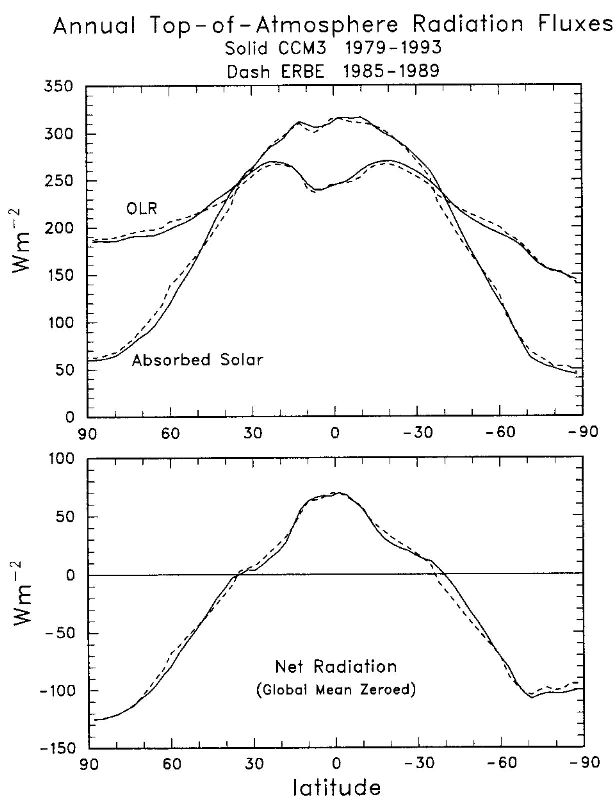

FIG. 13. Annual-mean, zonal-mean top-of-atmosphere outgoing longwave flux, absorbed shortwave flux, and net radiative flux (W m^{-2}) from the CCM3 (———) and the ERBE data (-----).

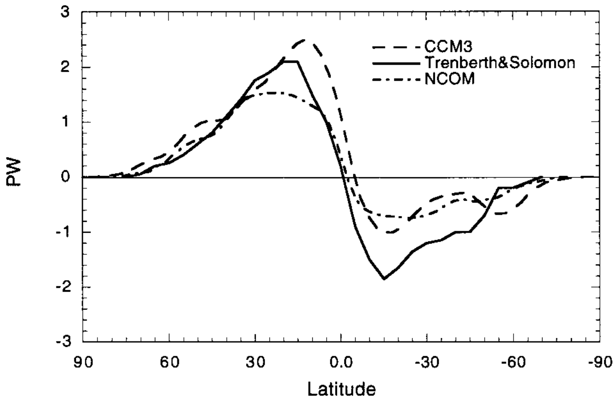

FIG. 14. Zonal mean of the implied ocean heat transport from CCM3 (– – –), the explicit ocean heat transport from NCOM (Gent et al. 1997 –·–·–), and the observational estimate of Trenberth and Solomon (1994) (———). Units are PW.

the CCM3 TOA energy budget and ERBE, which suggests that CCM3 should yield a reasonable simulation of the total poleward heat flux. Moreover, the agreement at the surface between the CCM3 and the Large et al. data suggests that good agreement should exist between the implied ocean heat transport and that obtained from the Large et al. data. Figure 14 shows the implied ocean heat transport from CCM3 and the observationally derived estimate from Trenberth and Solomon (1994). We also include the explicitly calculated ocean heat transport from the NCAR ocean model. There is good agreement between the CCM3 implied heat transport and the explicit ocean transport. Agreement of either model with the observationally derived heat transport is not as good, especially in the Southern Hemisphere, but this is where the observations are less reliable. From a coupling point of view, the agreement in poleward heat transport between the CCM3 and the NCOM suggests little drift should occur due to differences in the component models, which is indeed the case (Boville and Gent 1998). Hack (1998) describes the causes for the improved simulation of implied ocean heat transport in CCM3.

4. Geographic energy distribution

Zonally averaged fluxes of energy are important in describing the meridional structure that plays an important role in poleward heat transport. However, the climate system is forced by the three-dimensional distribution of energy (Trenberth and Solomon 1994). Furthermore, zonal averaging can mask regional biases in energy fluxes. Thus, to better understand the CCM3 global energy budget, we present the geographic distribution of the various energy fluxes at both the top of the atmosphere and at the surface, and to summarize, we focus on the annual mean energy budget.

The geographic distribution of the annual mean outgoing longwave flux from the CCM3 and the ERBE data is shown in Fig. 15. The three centers of low outgoing longwave flux associated with tropical deep convection and extensive anvil cloud systems are present in CCM3, but the model CCM3 produces too vigorous convection in the eastern Pacific basin, which results in a significant OLR bias. In the western Pacific, the model minima in OLR is located east of Borneo and New Guinea, whereas the ERBE data show these minima located over these island regions. Over the subtropical oceans the simulated OLR maxima are too large, and this bias is related to the clear sky outgoing longwave flux (Fig. 16). This bias in relatively dry regions is the same as discussed above for the downward flux; that is, the CCM radiation model underestimates the opacity of the atmosphere for low water vapor conditions.

The top-of-atmosphere annual mean shortwave absorbed flux from CCM3 and ERBE is shown in Fig. 17. The agreement between the CCM3 and the observations is good, with biases generally being less than 10 W m^{-2}. Kiehl (1998) discusses these biases in more detail for the tropical Pacific region. The radiative effect of clouds is best evaluated in terms of the cloud radiative forcing (Figs. 18 and 19). Biases in LWCF are apparent in the position of the convective systems in the western tropical Pacific, where the maximum in CCM3 is located east of New Guinea compared to over Borneo in the ERBE data. The LWCF in the eastern equatorial Pacific is too large in CCM3 compared to ERBE. There is good agreement ($<$10 W m^{-2}) between model and observations in both the South Pacific and South Atlantic convergence zones.

The overestimation of SWCF in the subtropical regions, especially in the south Pacific, is apparent in Fig. 19. The total cloud fraction in these regions is 20%, which is in agreement with the climatology of Warren et al. (1988) (also see Fig. 10). Thus, the source of this bias is more likely an overestimate of cloud water. The model precipitable water in this region is too large compared to observations (see Hack et al. 1998). Since, the cloud water is diagnosed from the precipitable water, there is an indication that the cloud water in this region may be overestimated, which would lead to an overestimate of cloud albedo. However, some of this bias could be a result of using a random overlap assumption for convective clouds. A maximum overlap assumption is perhaps more appropriate for the trade cumuli, which would lower the albedo of these clouds.

The geographic distribution of the annual mean net energy flux for CCM3 and the Large et al. (1997) data is shown in Fig. 20. There is remarkable agreement in the spatial patterns of net energy flux into the oceans (positive) and net energy flux from the ocean into the atmosphere (negative). The model simulates the input of energy into the equatorial region, but over estimates this flux in the Indian Ocean region compared to the Large et al. data. The large energy loss from the ocean off the eastern coasts of North America and Russia are simulated quite well. In the Southern Hemisphere, the CCM3 heat flux into the ocean is larger in the South

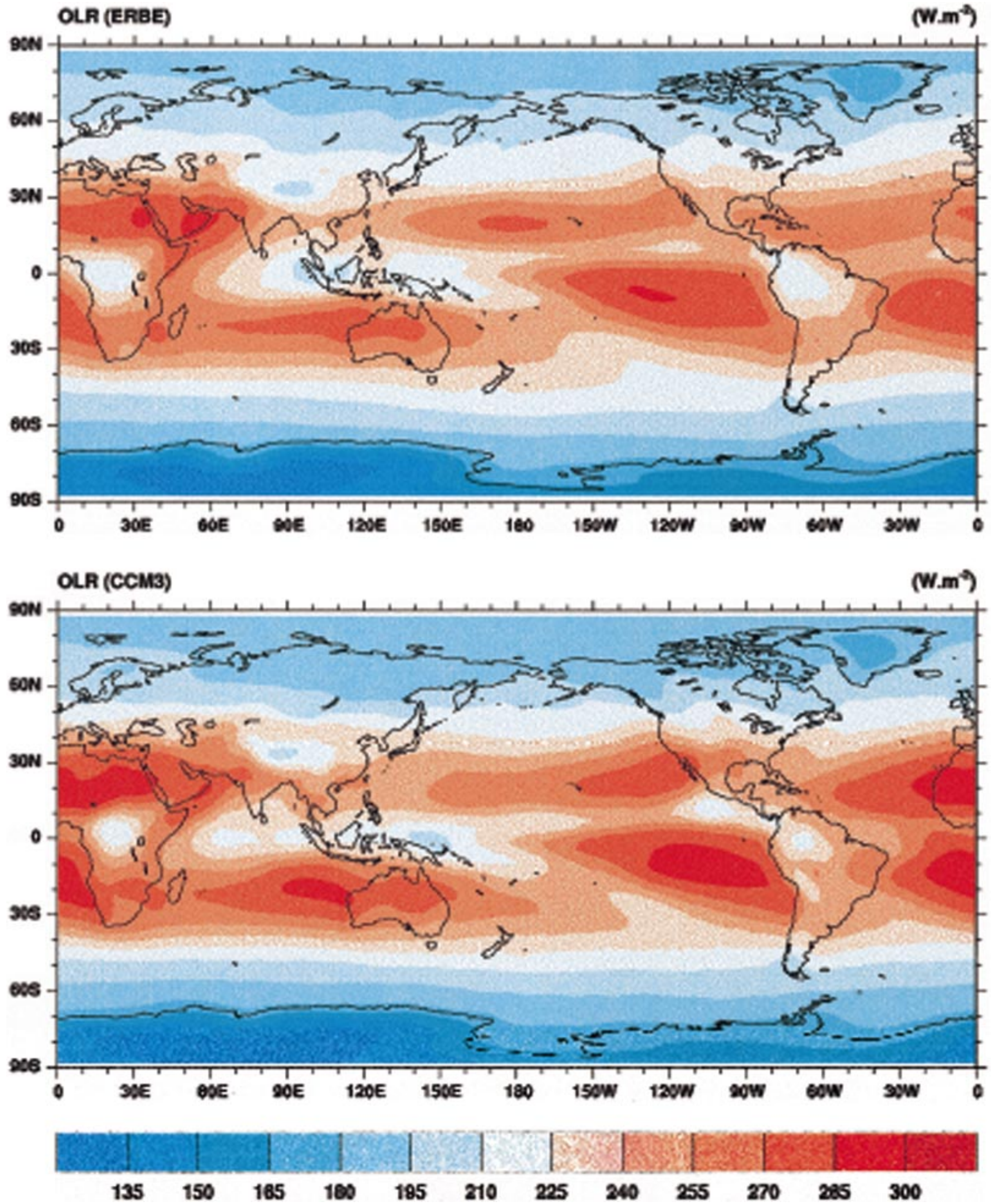

FIG. 15. Geographic distribution of ensemble-mean, annual-mean outgoing longwave flux (W m^{-2}) from (a) ERBE and (b) CCM3.

Atlantic region, than is estimated in the Large et al. data. A significant bias exists in the net energy flux into the eastern boundaries of the Pacific and Atlantic Oceans associated with the a poor simulation of coastal cloud in the CCM3. In particular, the CCM3 underestimates the cloud fraction of marine stratus and the resulting energy flux bias has serious implications for the CSM simulations.

Similar to the net energy flux, there is remarkable agreement in the spatial distribution of latent heat flux between the Large et al. data and the CCM3 (Fig. 21). The equatorial minima in latent heat flux are simulated quite well, including the eastern Pacific local minimum located over the cold tongue. Latent heat fluxes in the subtropical regions are larger in the model than in the Large et al. results due to an overestimate of the strength of the trade winds in CCM3 (see Hurrell et al. 1998).

The third largest energy flux that contributes to the net ocean surface flux is the net longwave flux (Fig. 22). The large longwave cooling near the eastern boundaries of the Pacific and Atlantic Oceans in the CCM3 is due to the lack of marine stratus cloud. The missing

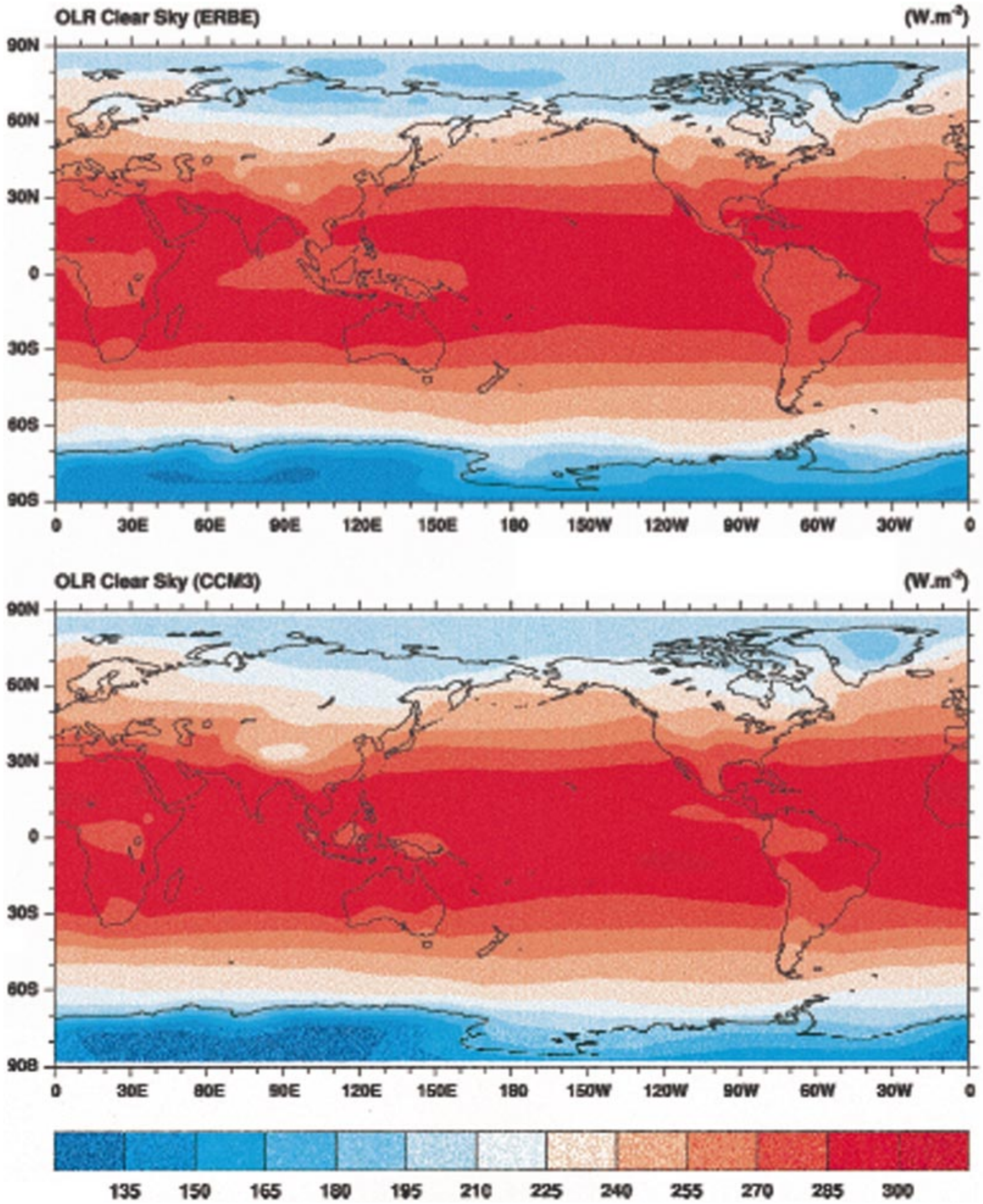

FIG. 16. Geographic distribution of ensemble-mean, annual-mean clear sky outgoing longwave flux (W m^{-2}) from (a) ERBE and (b) CCM3.

clouds in these regions produce small downward longwave fluxes; thus the net flux is too large. The most significant difference between the Large et al. results and the CCM3 is located between 20° and 40° in both hemispheres. As discussed in section 3, this bias is related to differences in total cloud cover between CCM3 and ISCCP, which is used in determining the Large et al. longwave fluxes. Thus, this difference in cloud cover is the source of the difference in longwave fluxes. Given the simplicity of the formulation used in the Large et al. longwave flux, we cannot assign a quantitative estimate of the bias between the CCM3 and Large et al. for this energy flux term. A more careful analysis of the approximation employed in the Large et al. data is required.

The last term in the net surface energy flux is the sensible heat flux (Fig. 23). The agreement in quite good between Large et al. and CCM3 in the regions off the east coasts of North America and Russia. However, over much of the open oceans, the CCM3 sensible heat flux is in general between 10 and 20 W m^{-2}, while the Large et al. fluxes are less than 10 W m^{-2}. The bias is most

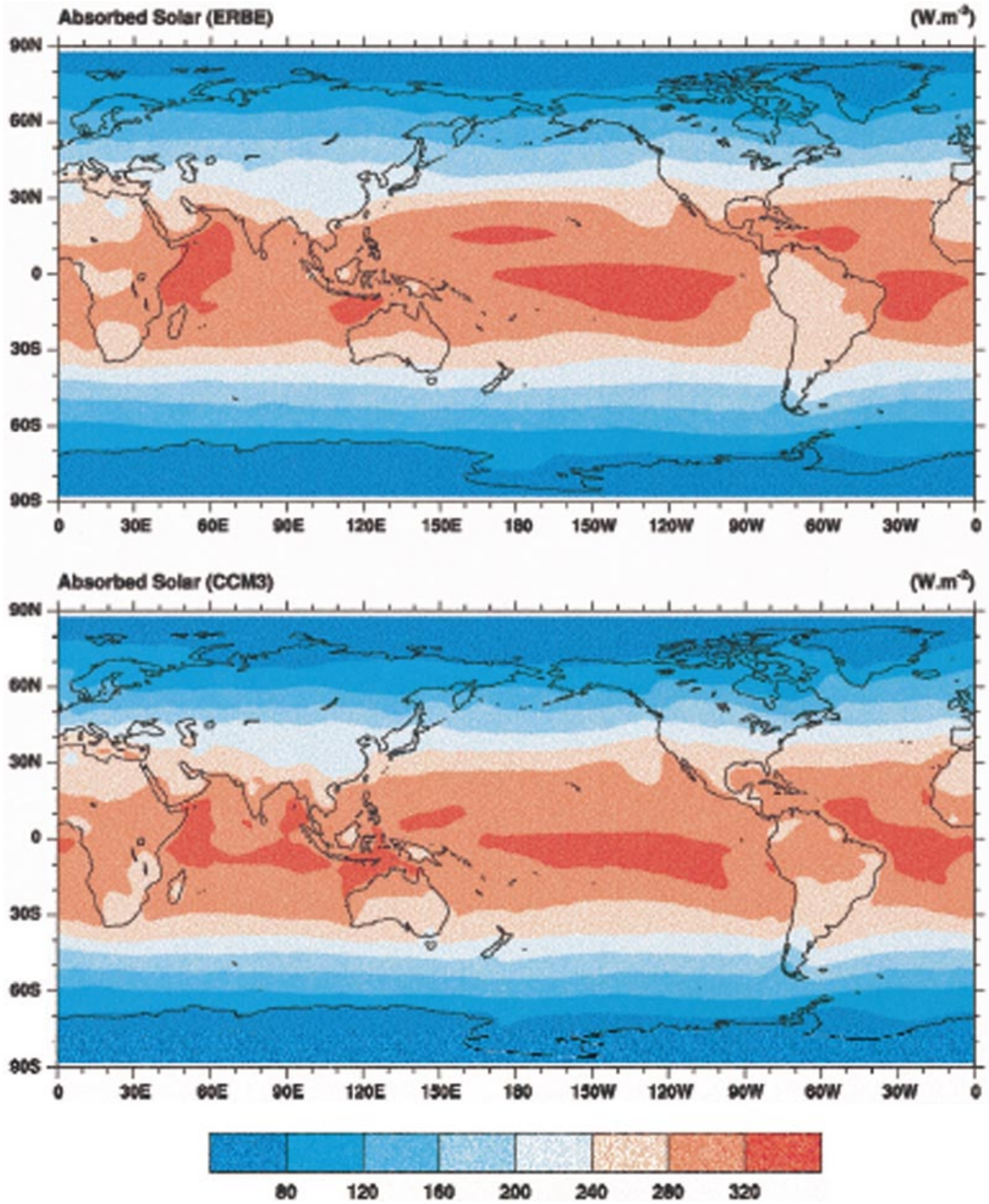

FIG. 17. Geographic distribution of ensemble mean, annual-mean shortwave absorbed flux (W m^{-2}) from (a) ERBE and (b) CCM3.

pronounced in the subtropics and is, no doubt, again related to biases in surface wind speed (Hurrell et al. 1998).

5. Seasonal regional analyses

So far we have considered seasonal and annual mean averages of the energy fluxes. To gain a better understanding of the CCM3 simulation of the energy budget, we now focus on the seasonal cycle of the energy fluxes for specific regions. We will consider regions over both ocean and land.

a. North Atlantic

The North Atlantic region is defined as open ocean in the domain between 30°–50°N and 60°–10°W. The energy fluxes in this region are strongly affected by the North Atlantic storm track cloudiness (Weaver and Ramanathan 1996). Figure 24 shows the seasonal cy-

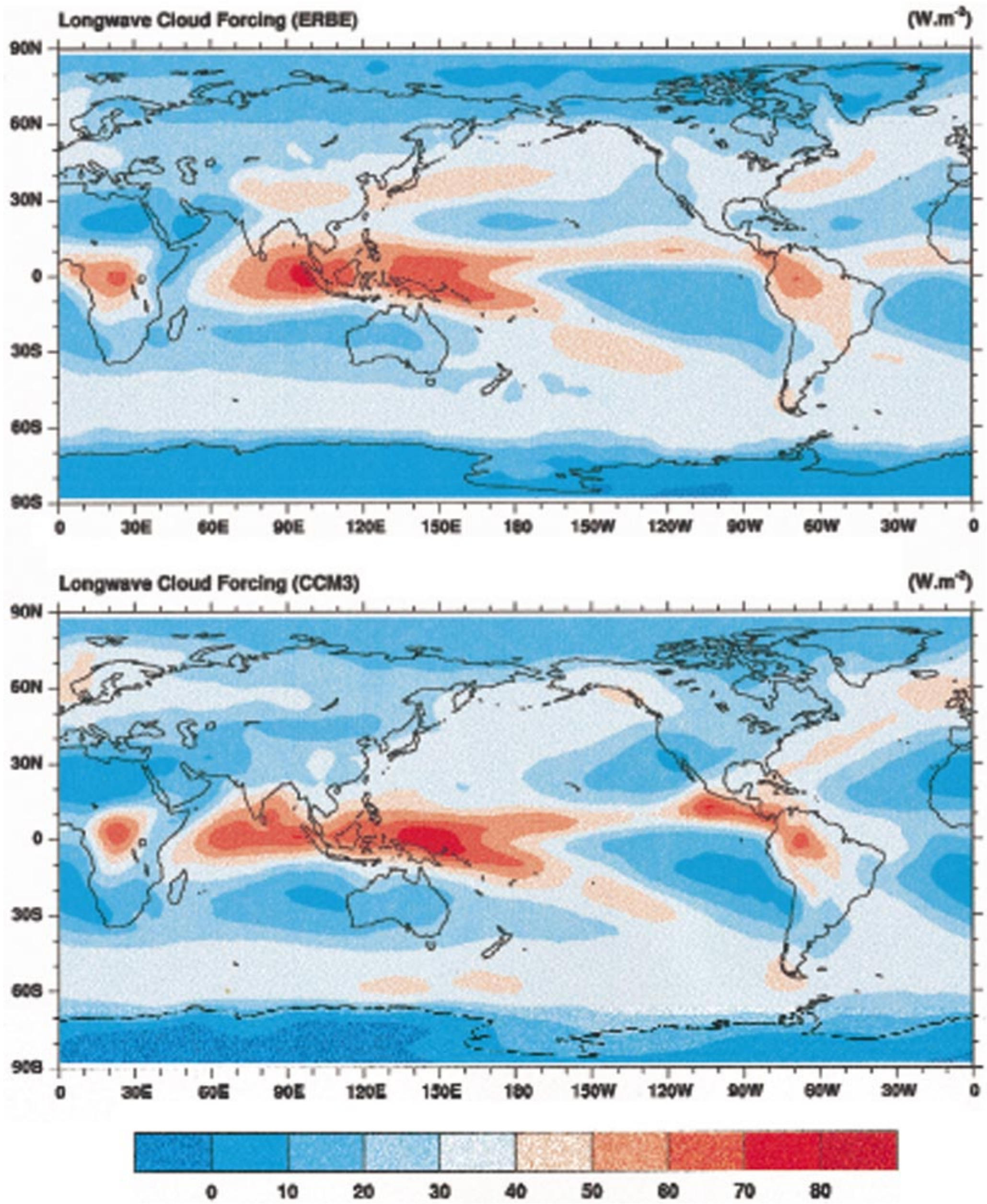

FIG. 18. Geographic distribution of ensemble-mean annual-mean longwave cloud forcing (W m^{-2}) from (a) ERBE and (b) CCM3.

cle of the dominant terms in the top-of-atmosphere and surface energy fluxes. At the top of the atmosphere, there is excellent agreement in both phase and amplitude between the CCM3 and ERBE seasonal cycle in shortwave absorbed fluxes. In the outgoing longwave fluxes there is also very good agreement (differences less than 4 W m^{-2}). At the surface, the two dominant energy fluxes are the net shortwave and latent heat flux. Figures 24c,d indicate that the CCM3 predicts an excess of shortwave flux reaching the ocean surface, in spite of the excellent agreement at the top of the atmosphere. As mentioned before, this must be a result of the underestimation of shortwave cloud absorption. Note that the model yields very good agreement with the satellite-derived surface fluxes from Bishop and Rossow (1991), but these fluxes were found to be too high when compared to ship observations by Large et al. (1997). The seasonal cycle of latent heat flux for the CCM3 (Fig. 24d) is in excellent agreement both in phase and amplitude with

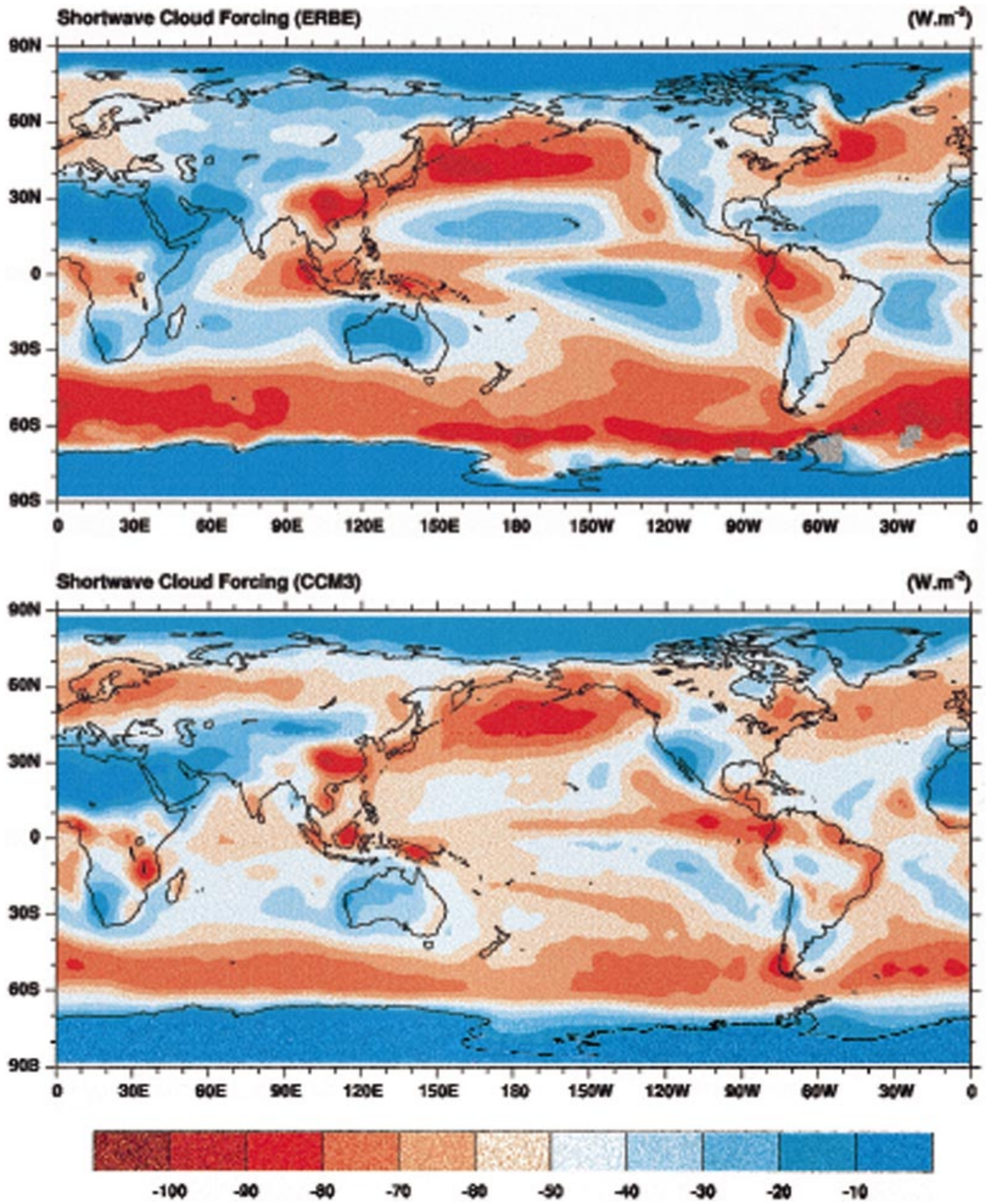

FIG. 19. Geographic distribution of ensemble-mean, annual-mean shortwave cloud forcing (W m^{-2}) from (a) ERBE and (b) CCM3.

the Large et al. results. Thus, for the North Atlantic region the TOA and surface energy fluxes are in very good agreement with observations, excluding the shortwave at the surface.

b. North Pacific

The North Pacific region is defined as that bounded by 30°–50°N and 150°E–140°W. This region is also dominated by storm track cloudiness and is thus of climatic importance (Weaver and Ramanathan 1996). As in the North Atlantic region there is excellent agreement in both phase and amplitude of the top-of-atmosphere shortwave absorbed flux (Fig. 25a). For the outgoing longwave flux the largest biases are within the ±7 W m^{-2} uncertainty of regional ERBE fluxes (Harrison et al. 1990) including the largest bias of 7 W m^{-2} in February. At the surface, similar to the North Atlantic region, there is a significant bias in the net shortwave flux (Fig. 25c), but there is excellent agreement in both phase and amplitude for the latent heat flux (Fig. 25d).

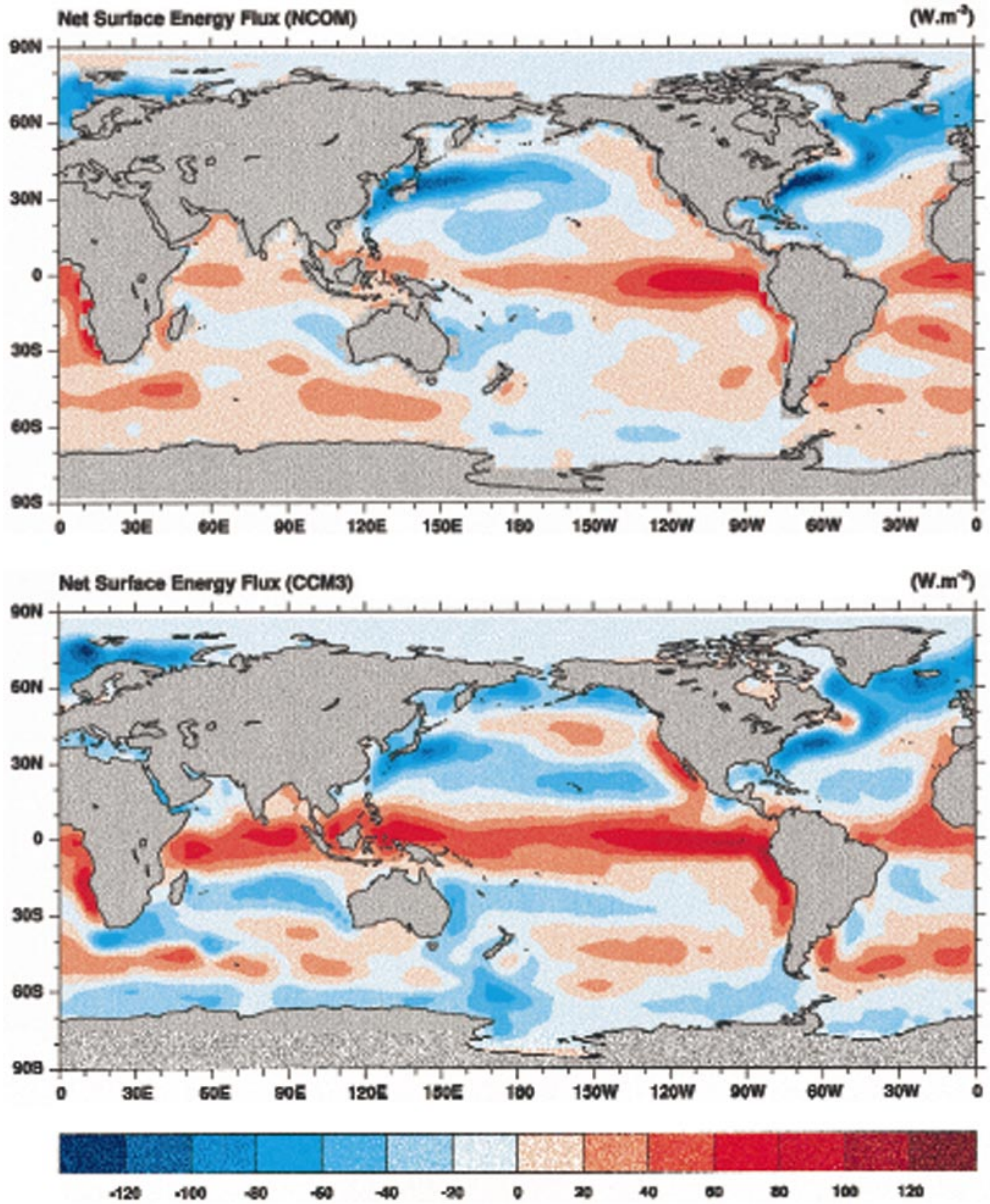

FIG. 20. Geographic distribution of ensemble-mean, annual-mean net surface energy flux (W m^{-2}) from (a) Large et al. and (b) CCM3.

c. *Warm pool*

The simulation of the annual mean energy budget of the warm pool region (10°S–10°N; 140°–170°E) is discussed by Kiehl (1998). The focus here is on the seasonal cycle of the dominant energy flux terms (Figs. 26a–d). At the top of the atmosphere, there is good agreement (differences less than 10 W m^{-2}) between the CCM3 and ERBE absorbed shortwave fluxes. The largest bias occurs between January and March, where the CCM3 flux is too large. This bias is related to the positioning of convective activity at this time of the year. The CCM3 places the convection too far east and south of the observed position (Hack et al. 1998). The outgoing longwave fluxes agree to within 5 W m^{-2} for all months except February, when the CCM3 OLR is almost 10 W m^{-2} larger than the ERBE value. Again this is an indication of the lack of convective activity in the warm pool region during this month of the year. At the surface, the bias in net shortwave flux is quite large (~35 W m^{-2}), where CCM3 overestimates this flux

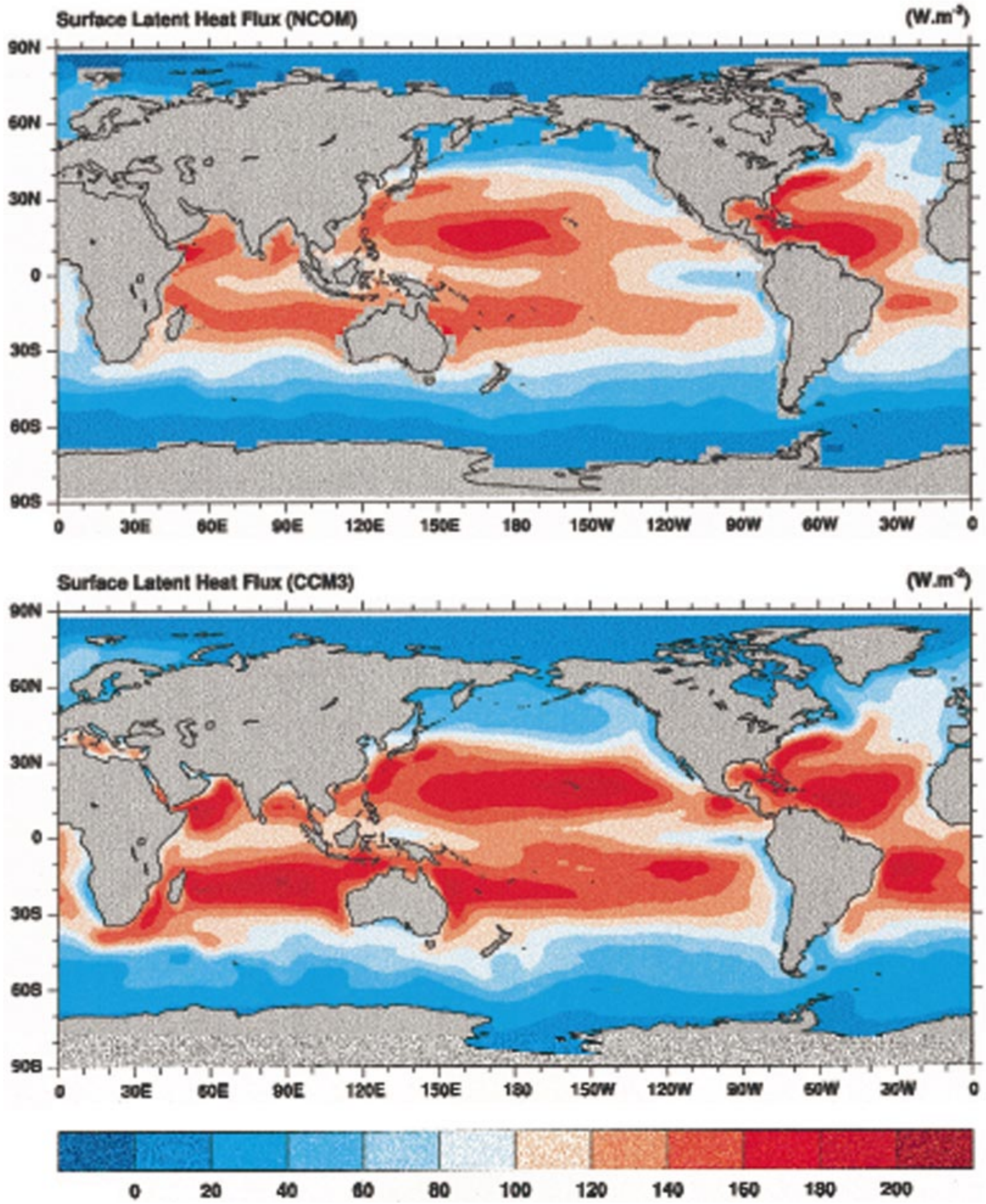

FIG. 21. Geographic distribution of ensemble-mean, annual-mean latent heat flux (W m^{-2}) from (a) Large et al. and (b) CCM3.

compared to both Large et al. and direct measurements (Kiehl 1998). The magnitude of the bias is similar to that discussed by Ramanathan et al. (1995) for this region, which they attributed to enhanced cloud absorption. For the latent heat flux, Fig. 25d shows very good agreement between the CCM3 and Large et al. This order of agreement was also found by CO97 for the western and central equatorial Pacific in comparisons between CCM3 and TOGA-TAO array-derived latent heat fluxes.

d. Peruvian coast

As previously discussed, the CCM3 simulation of marine stratus clouds in CCM3 is deficient along the eastern boundaries of the Pacific and Atlantic coastal regions. To explore this bias in more detail, we present the seasonal cycle of terms in the TOA and surface energy budget for a region off the coast of Peru (20°–10°S, 90°–80°W) (Fig. 27a). From June to December there is a significant (20 W m^{-2}) bias in the top-of-

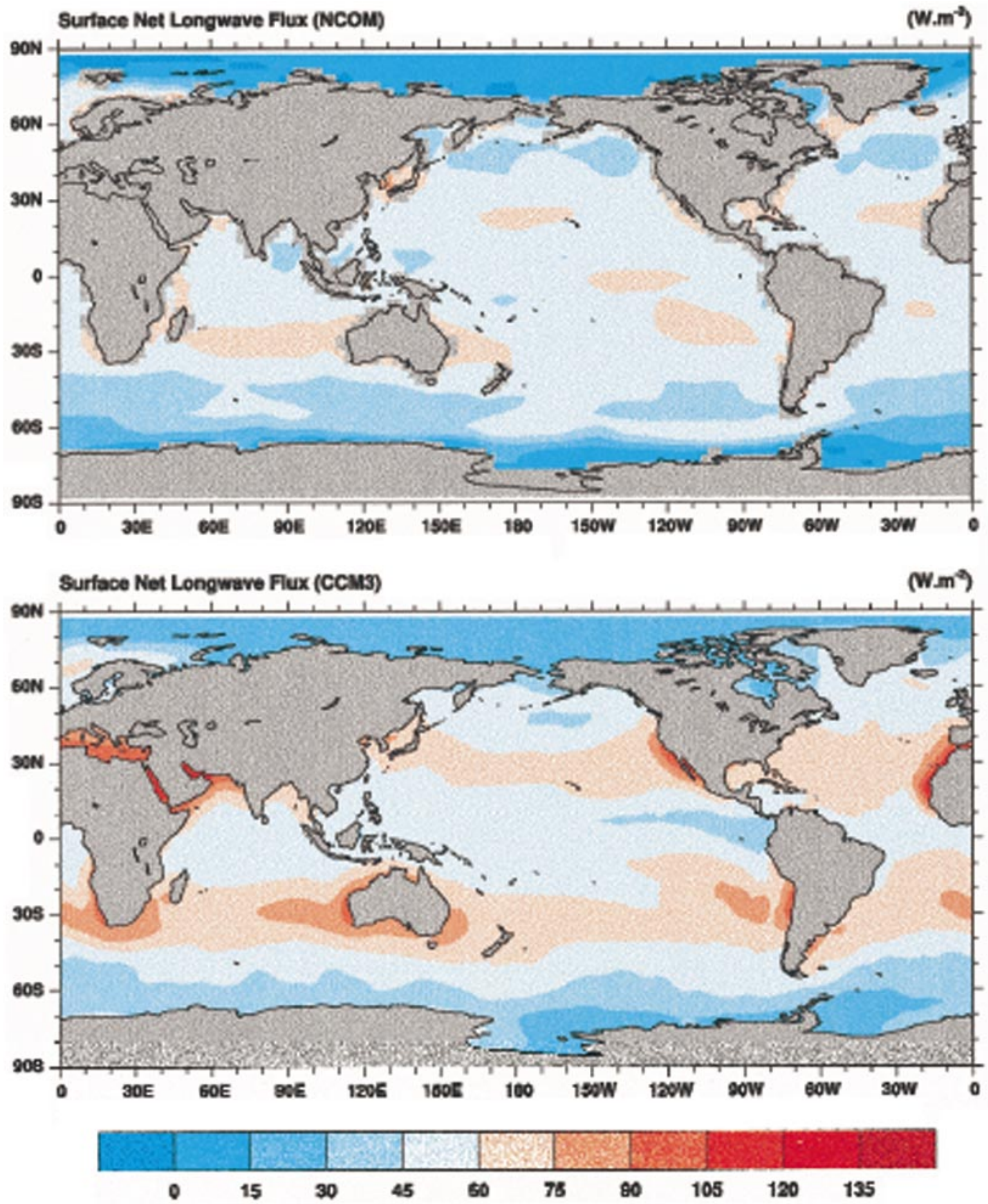

FIG. 22. Geographic distribution of ensemble-mean, annual-mean net longwave flux (W m^{-2}) from (a) Large et al. and (b) CCM3.

atmosphere shortwave flux, where the CCM3 flux is larger than observed. This excess in absorbed flux is due to a lack of stratus cloud during these months in the CCM3. Figure 28 compares the seasonal cycle in low-level cloud cover from CCM3 with the observational results employed by Klein and Hartmann (1993). Note that the model has little seasonal cycle in low cloud cover, while the observations show a significant seasonal cycle in cloud cover. There is very little seasonal cycle in the outgoing longwave flux (Fig. 27b) in either the CCM3 or the ERBE data, but there is a 15 W m^{-2} difference between the model and the observations. At the surface, the bias in the net shortwave flux (Fig. 27c) is large due to both the lack of cloud cover during June–December and an underestimation in shortwave cloud absorption. This can be seen by comparing the bias for February–May to that of June–January. Figure 27d shows the seasonal cycle in latent heat flux from the CCM3 and the Large et al. data. The model agrees well for most months with the Large et al. results.

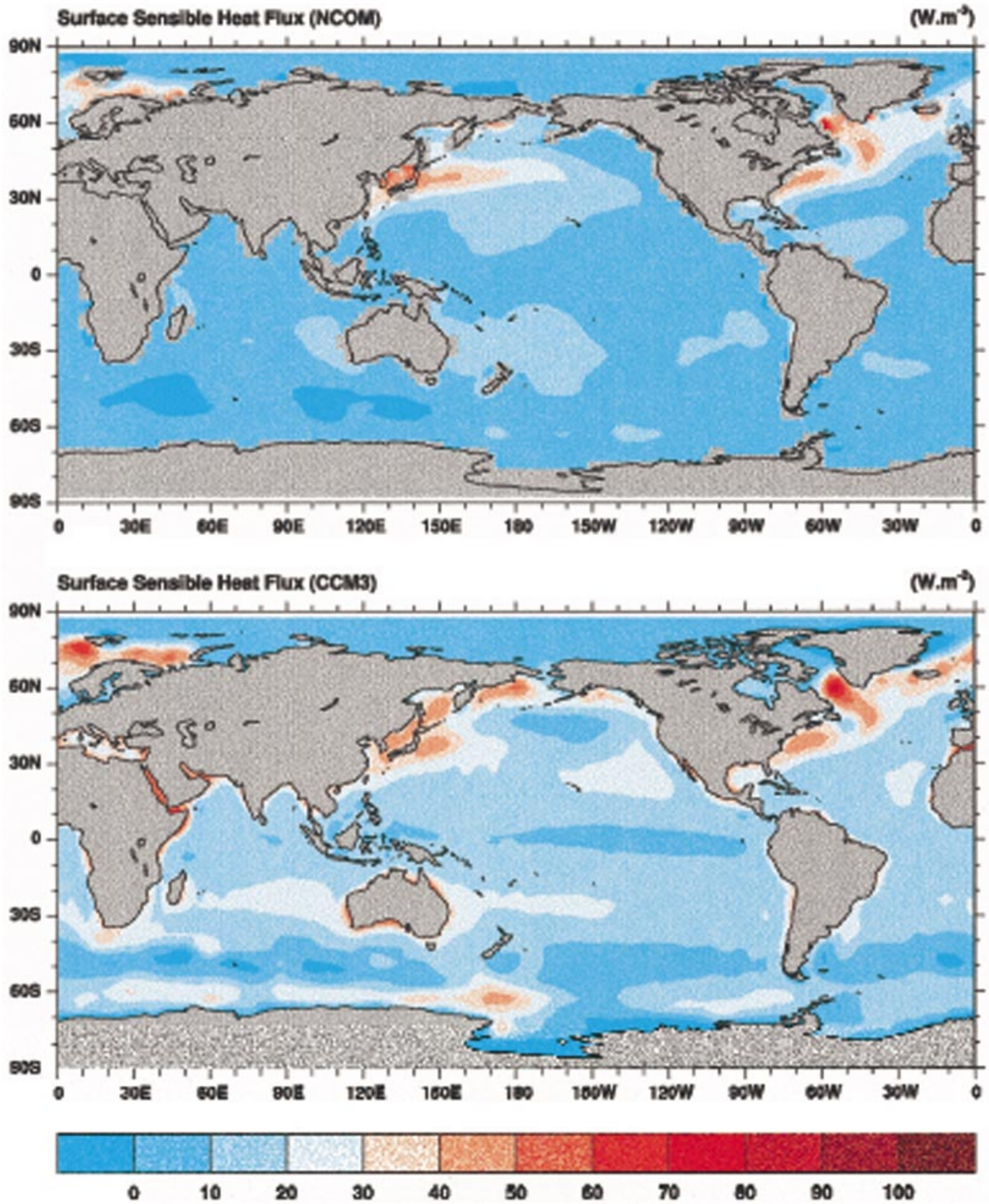

FIG. 23. Geographic distribution of ensemble-mean, annual-mean sensible heat flux (W m^{-2}) from (a) Large et al. and (b) CCM3.

e. Eastern United States

Over land regions we do not have access to a global seasonal climatology of surface fluxes, so we limit the comparison to top-of-atmosphere shortwave and longwave fluxes. In addition, regional seasonal analysis of surface fluxes over land is discussed by Bonan (1998). Figure 29a compares the seasonal cycle of these fields from CCM3 and ERBE for a region in the eastern United States (30°N, 50°N, 90°W, 70°W). The model and observations agree to within 10 W m^{-2} for most months. There is a one-month phase difference, where the ERBE absorbed flux peaks in June, while the model flux peaks in July. For most months the CCM3 flux is lower than ERBE, indicating the model albedo is higher than the observations. This bias was noted by Zhang et al. (1998) in their analysis of the shortwave fluxes over continents. Figure 29b shows the seasonal cycle of the outgoing longwave flux from CCM3 and ERBE. The one-month bias in phase is also apparent in the OLR.

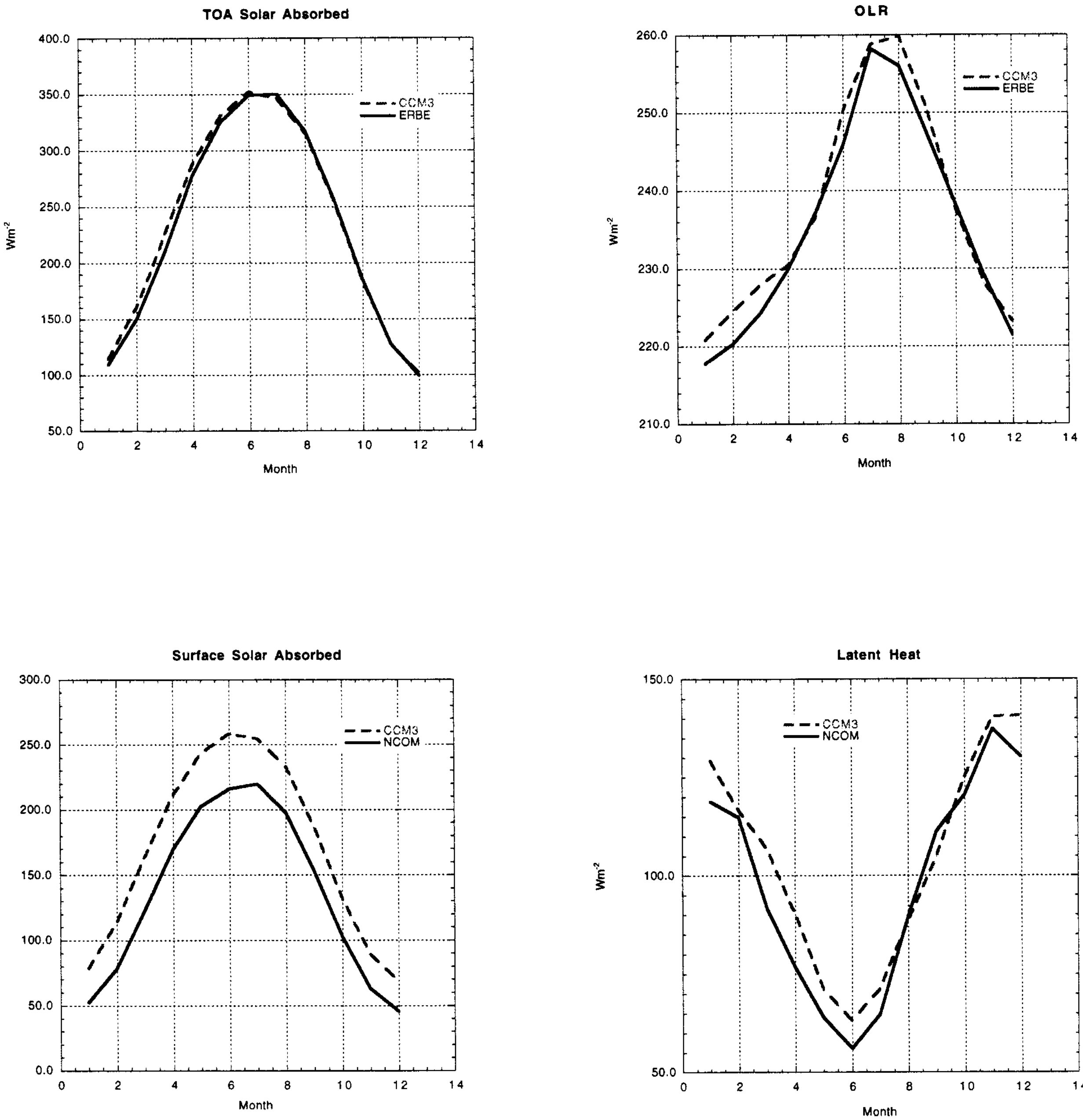

FIG. 24. Seasonal cycle for the North Atlantic region of the (a) TOA shortwave absorbed flux, (b) outgoing longwave flux from CCM3 (– – –) and ERBE (———), (c) surface shortwave absorbed flux, and (d) surface latent heat flux from CCM3 (– – –) and Large et al. (———). Fluxes are in units of W m^{-2}.

f. Central United States

The seasonal cycle in TOA fluxes for a region in the central United States (30°N, 50°N, 110°W, 90°W) is shown in Figs. 30a,b. There is excellent agreement between the TOA shortwave absorbed fluxes between the model and ERBE. The biases in the seasonal cycle of the OLR (Fig. 30b) are fairly large ($\sim$25 W m^{-2}) during June and July, where the observed OLR is less than the model result. This result, combined with the shortwave result, suggests that the model is not simulating upper-level cloud due to summer convective activity, but is simulating total cloud cover (which strongly affects the shortwave) reasonably well.

g. Central Europe

The biases in the seasonal cycle of TOA shortwave and longwave fluxes for a region in central Europe

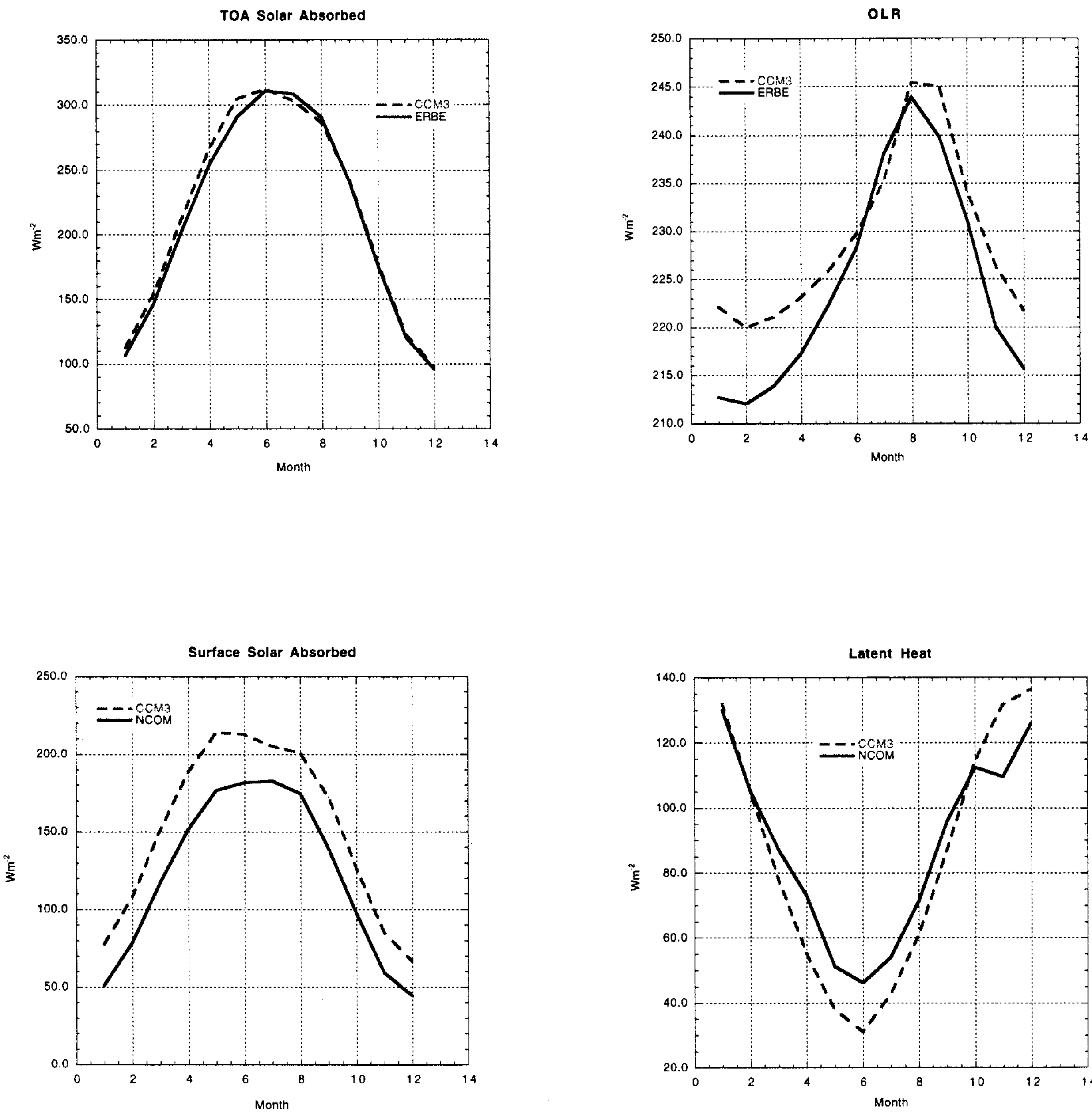

FIG. 25. Seasonal cycle for the North Pacific region of the (a) TOA shortwave absorbed flux, (b) outgoing longwave flux from CCM3 (– – –) and ERBE (———), (c) surface shortwave absorbed flux, and (d) surface latent heat flux from CCM3 (– – –) and Large et al. (———). Fluxes are in units of W m^{-2}.

(40°N, 55°N, 10°W, 40°E) (Figs. 31a,b) look quite similar to the those for the central United States. There is very good agreement in the shortwave, while the agreement in the OLR is not as good. Note that the disagreement in the OLR (Fig. 31b) is mainly due to a one-month phase lag between the CCM3 and ERBE. Since the shortwave flux does not exhibit this phase shift problem, one possible explanation for this is that the seasonal cycle in model surface temperature in this region is phase shifted by one month.

h. Amazon

In the Tropics, a region of particular climatic interest is the Amazon (10°S, 0°, 70°W, 50°W), in view of the rapid tropical deforestation in this region. Figures 32a,b show the seasonal cycle in TOA absorbed shortwave and OLR from the CCM3 and ERBE. The observed fluxes exhibit a signature of the seasonal cycle in convection for this region. During Southern Hemisphere summer, convective activity is located

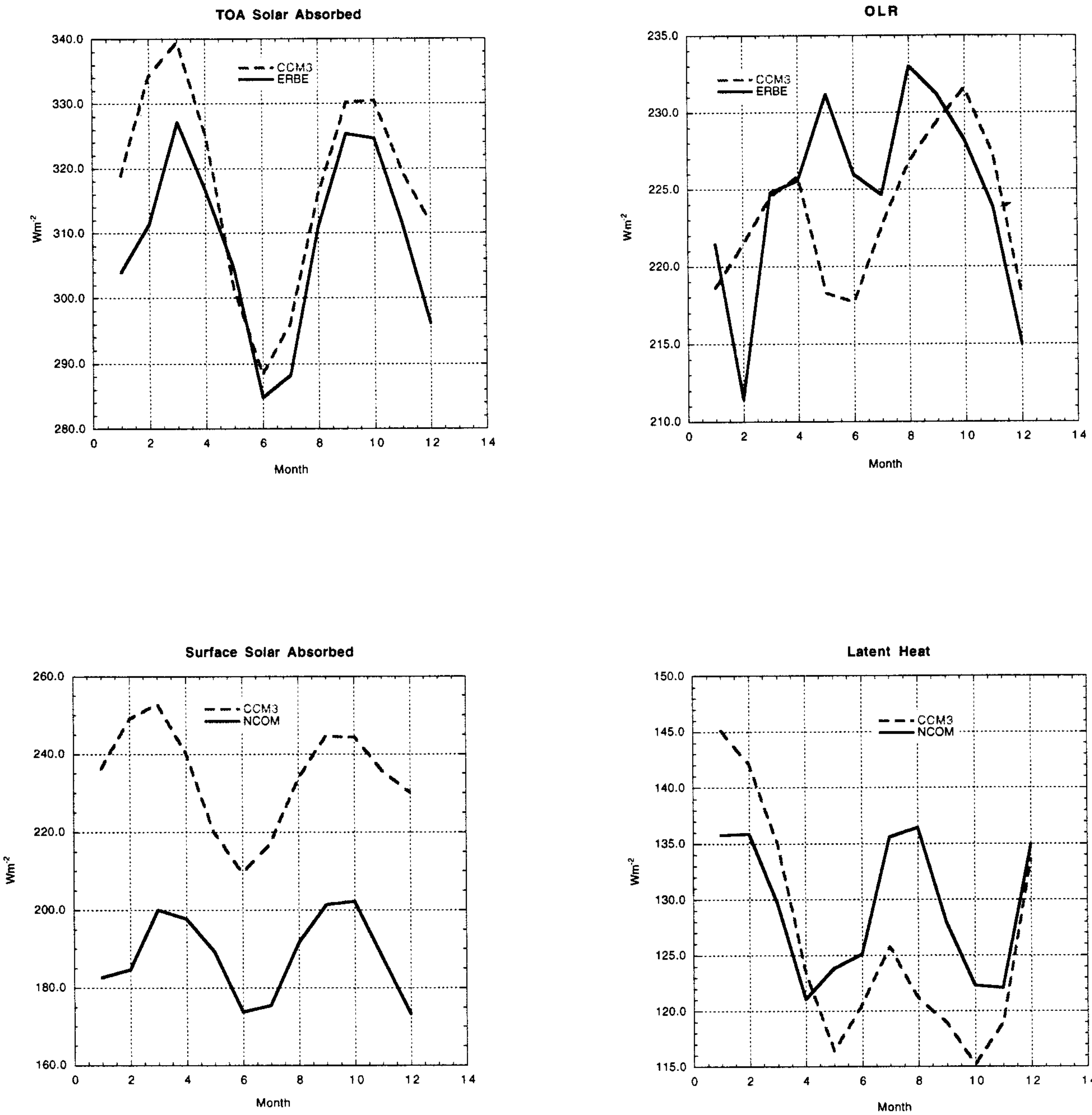

FIG. 26. Seasonal cycle for the warm pool region of the (a) TOA shortwave absorbed flux, (b) outgoing longwave flux from CCM3 (– – –) and ERBE (———), (c) surface shortwave absorbed flux, and (d) surface latent heat flux from CCM3 (– – –) and Large et al. (———). Fluxes are in units of W m^{-2}.

over this region, while during local winter the convection migrates north to central America. Thus, the OLR is low (absorbed shortwave is low) during local summer, whereas OLR is high (absorbed shortwave is high) during local winter. A bias in OLR of ~20 W m^{-2} from January–August is indicative of the underprediction of upper-tropospheric cloud properties (e.g., condensate and/or cloud fraction). In the shortwave, there is a large bias in local summer absorbed shortwave, where the model's convective clouds are less reflective than observations indicate. This could be related to the scale height assumption employed for cloud condensate (Hack 1998).

i. Congo

Another tropical land region of great interest is that of the central Africa (10°S, 5°N, 10°E, 30°E) (Figs. 33a,b). Except for July and August, there is very good agreement in absorbed shortwave flux (<10 W m^{-2})

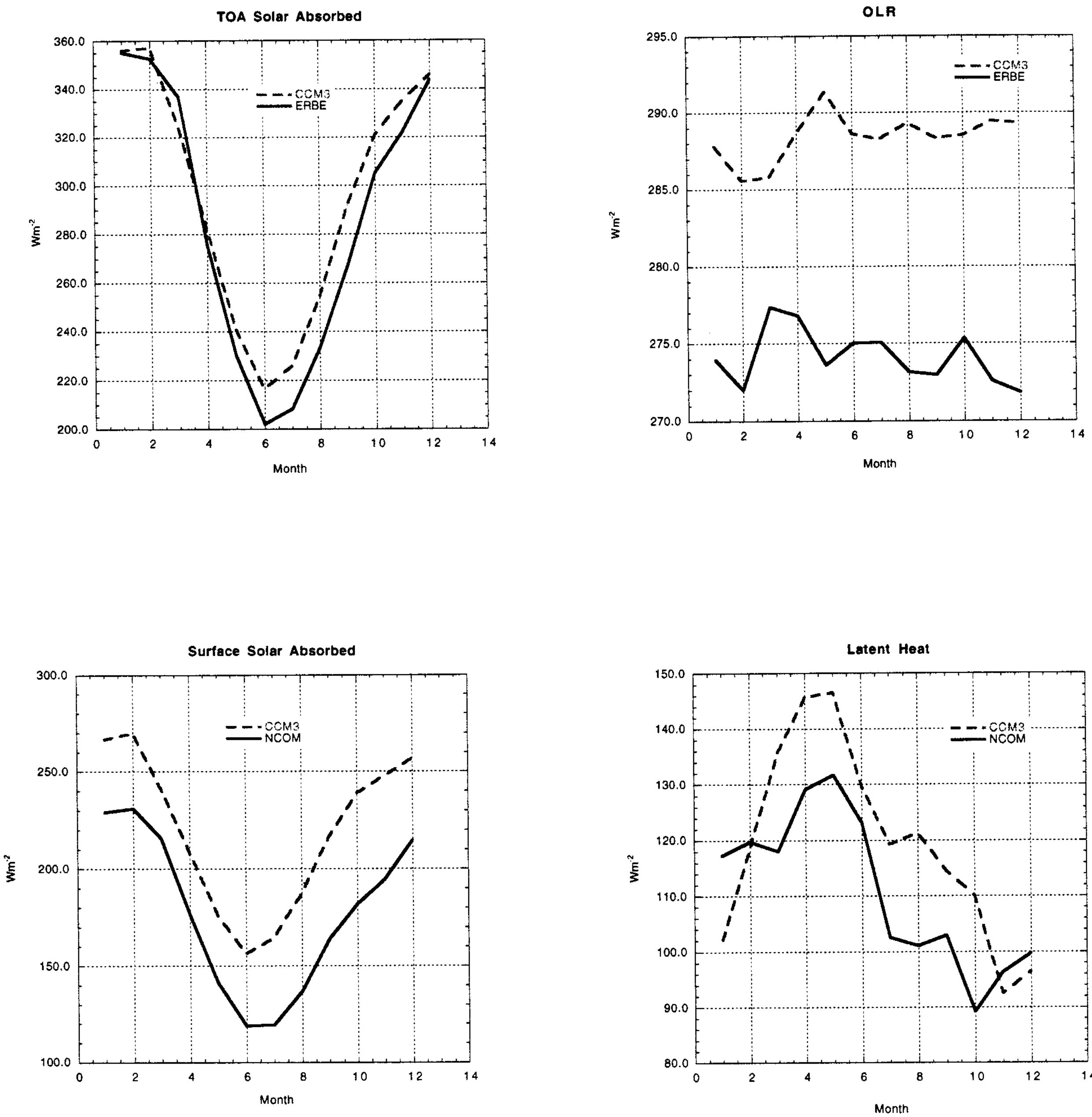

FIG. 27. Seasonal cycle for the Peruvian coastal region of the (a) TOA shortwave absorbed flux, (b) outgoing longwave flux from CCM3 (– – –) and ERBE (———), (c) surface shortwave absorbed flux, and (d) surface latent heat flux from CCM3 (– – –) and Large et al. (———). Fluxes are in units of W m^{-2}.

between CCM3 and ERBE. The disagreement for OLR is much larger, with differences from March through June as large as 30 W m^{-2}.

6. Transient response

The results presented so far have dealt with the time-mean climatology of the model, from monthly, seasonal, to annual timescales. The simulations of the CCM3 are forced with observed monthly mean SSTs from 1979 to 1994. During this time period, tropical sea surface temperatures undergo significant interannual variability due to the El Niño–Southern Oscillation (ENSO) phenomena, and the anomalous SSTs provide significant forcing for atmospheric models (e.g., Chen et al. 1995). The responses in the TOA earth radiation budget have also been documented from observations, so the ability of an atmospheric climate model to reproduce these responses is a necessary test.

We consider two measures of the response of the

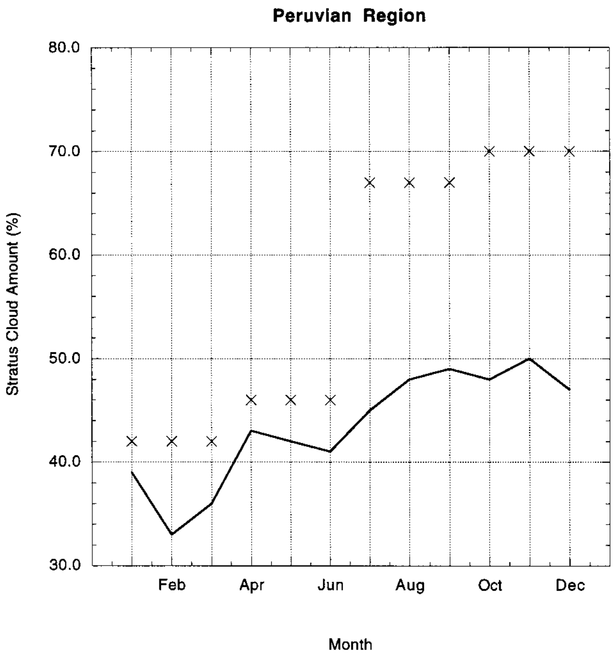

FIG. 28. Seasonal cycle in low cloud fraction (%) over the Peruvian region from CCM3 (———) and the observations from Klein and Hartmann (1993) (×).

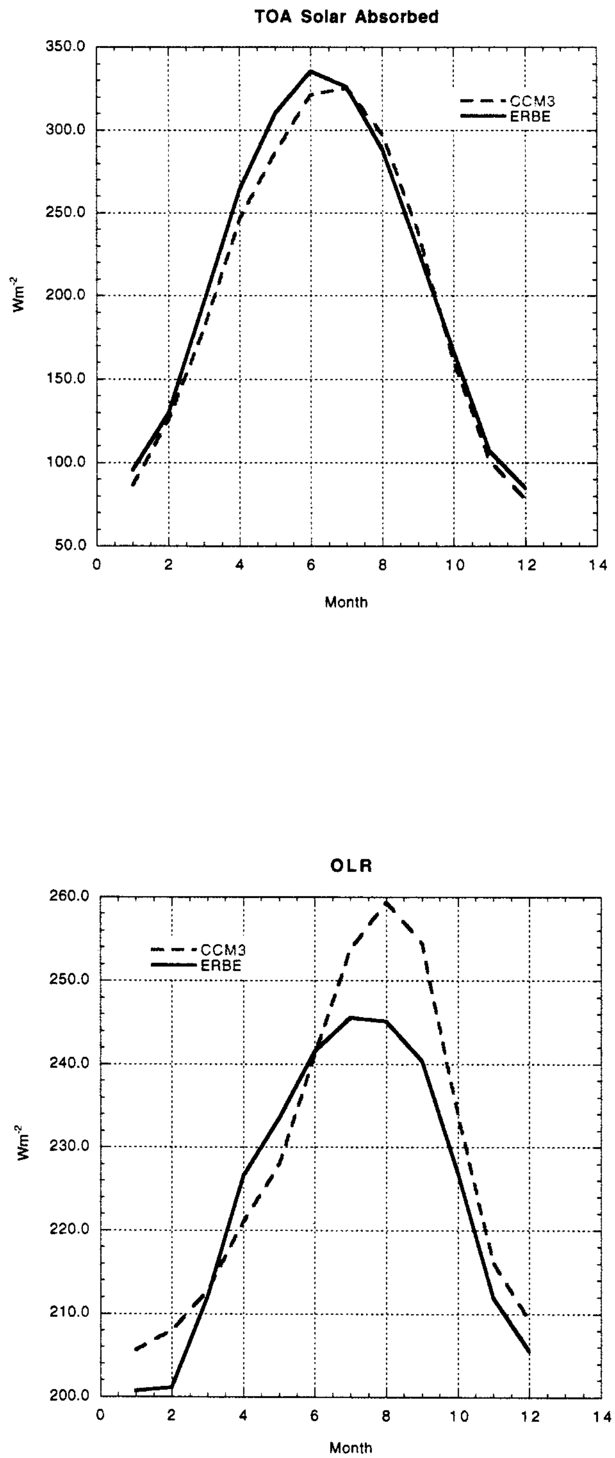

FIG. 29. Seasonal cycle for the eastern United States region of the (a) TOA shortwave absorbed flux and (b) outgoing longwave flux from CCM3 (– – –) and ERBE. Fluxes are in units of W m^{-2}.

CCM3 to anomalies in tropical SSTs. First, Fig. 34 shows a Hovmöller diagram of anomalies in OLR from 1979 to 1993 from the National Oceanic and Atmospheric Administration (NOAA) polar-orbiting satellites (Hurrell and Campbell 1992) and from the CCM3. The strong 1982–83 warm event is seen in both observations and the model. Notable is the positive anomaly in OLR centered between 120° and 140°E and the accompanying negative OLR anomaly between 160° and 120°W. This pattern is a result of an eastward shift in convective activity associated with the eastward propagation of warm water in the tropical Pacific. The model shows good agreement with this pattern for the 1982–83 warm event, although the positive anomaly in the CCM3 is slightly weaker than the observed. The reverse pattern exists during 1984–85, which was dominated by a La Niña. The next warm event occurred in 1987, and the model captures this response, but the positive anomaly in the western Pacific is not as coherent as the observed pattern. The third warm event occurs in the 1990s, which was a period of sustained warm anomalies in SST. The model simulates the response in OLR during this period.

A second way to study the response of the atmosphere to anomalies in SST is to consider the change in SWCF relative to the change in LWCF. The observations of this quantity in the Tropics show a strong linear anticorrelation between these two cloud forcings (see Ramanathan and Collins 1991; Kiehl 1994b). Figure 35 shows this correlation for the entire equatorial Pacific (10°S–10°N, 140°E–90°W) for both ERBE and the CCM3. The change in cloud radiative forcing is obtained by differencing March–May averages between 1987 (warm event) and 1985 (cold event). Linear fits to these data are shown for both the observations and

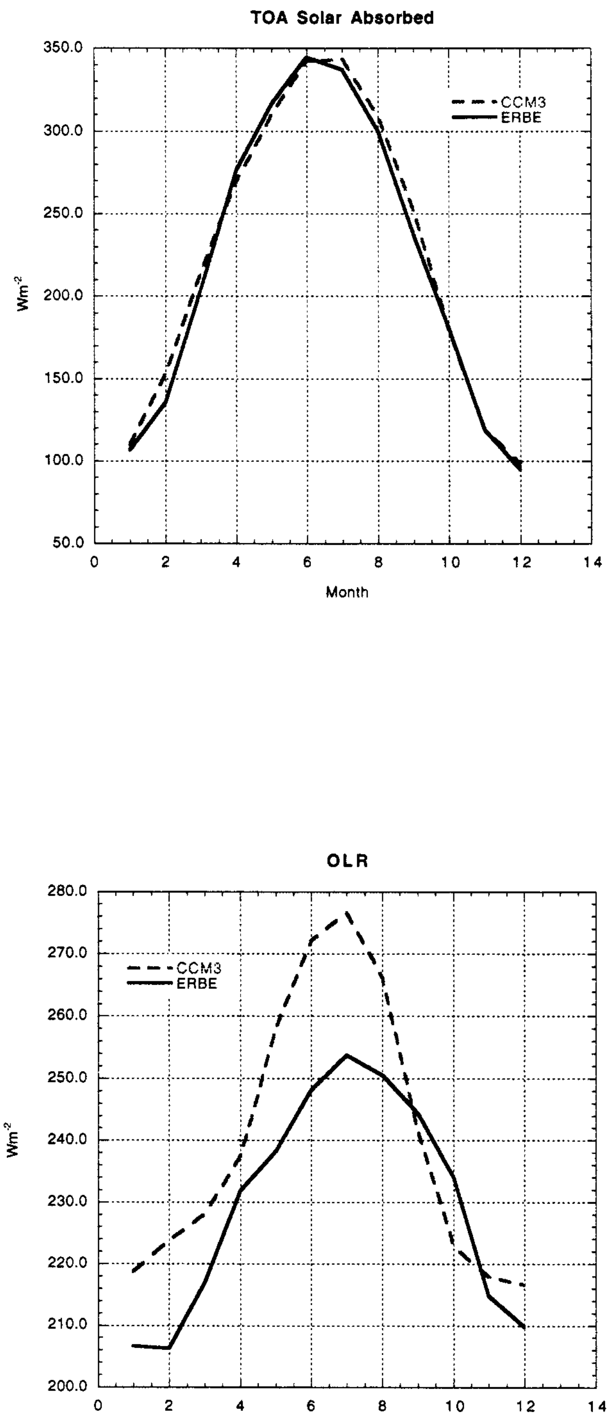

FIG. 30. Seasonal cycle for the central United States region of the (a) TOA shortwave absorbed flux and (b) outgoing longwave flux from CCM3 (– – –) and ERBE. Fluxes are in units of W m^{-2}.

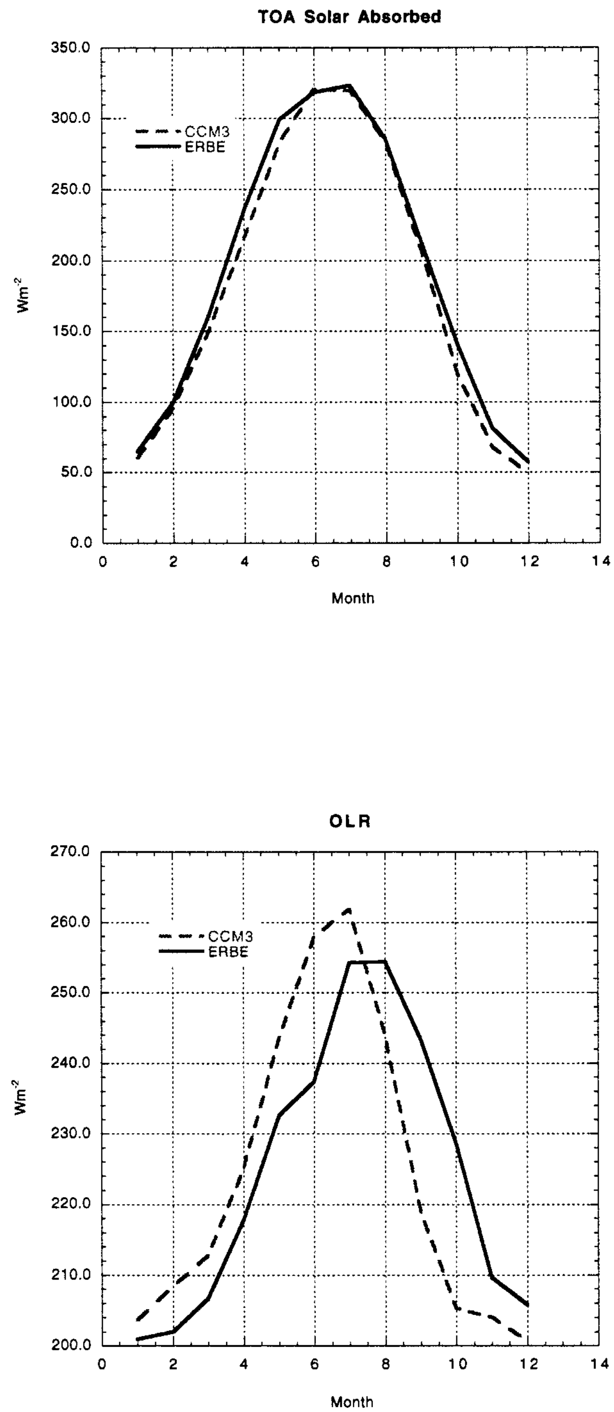

FIG. 31. Seasonal cycle for the central Europe region of the (a) TOA shortwave absorbed flux and (b) outgoing longwave flux from CCM3 (– – –) and ERBE. Fluxes are in units of W m^{-2}.

the CCM3. The ERBE data indicate a strong correlation between the δSWCF and δLWCF, with a slope of -1.23, that is, the change in SWCF is somewhat larger than the change in LWCF. The CCM3 predicts a weaker correlation between δSWCF and δLWCF, moreover, the standard deviation is much larger than observed, and the slope is only -0.5. This is in strong contrast to CCM2 and a version of CCM2 that employs the diagnostic cloud water scheme (see Hack 1998). The major

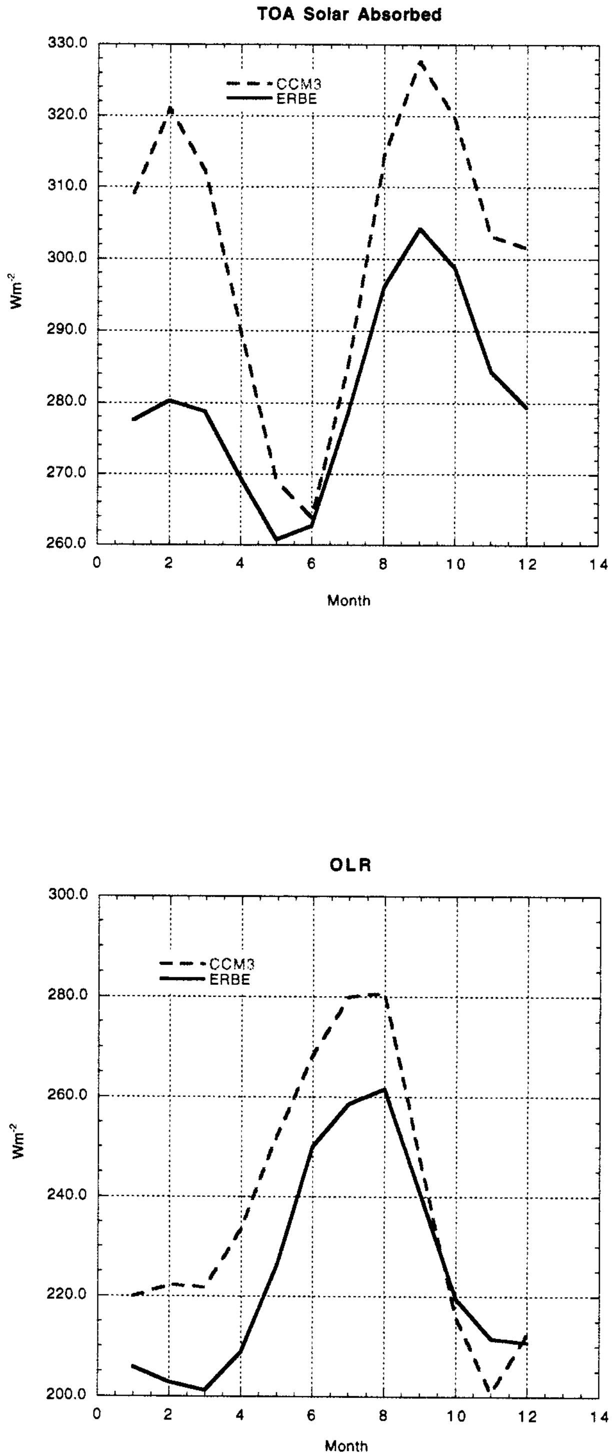

FIG. 32. Seasonal cycle for the Amazon region of the (a) TOA shortwave absorbed flux and (b) outgoing longwave flux from CCM3 (– – –) and ERBE. Fluxes are in units of W m^{-2}.

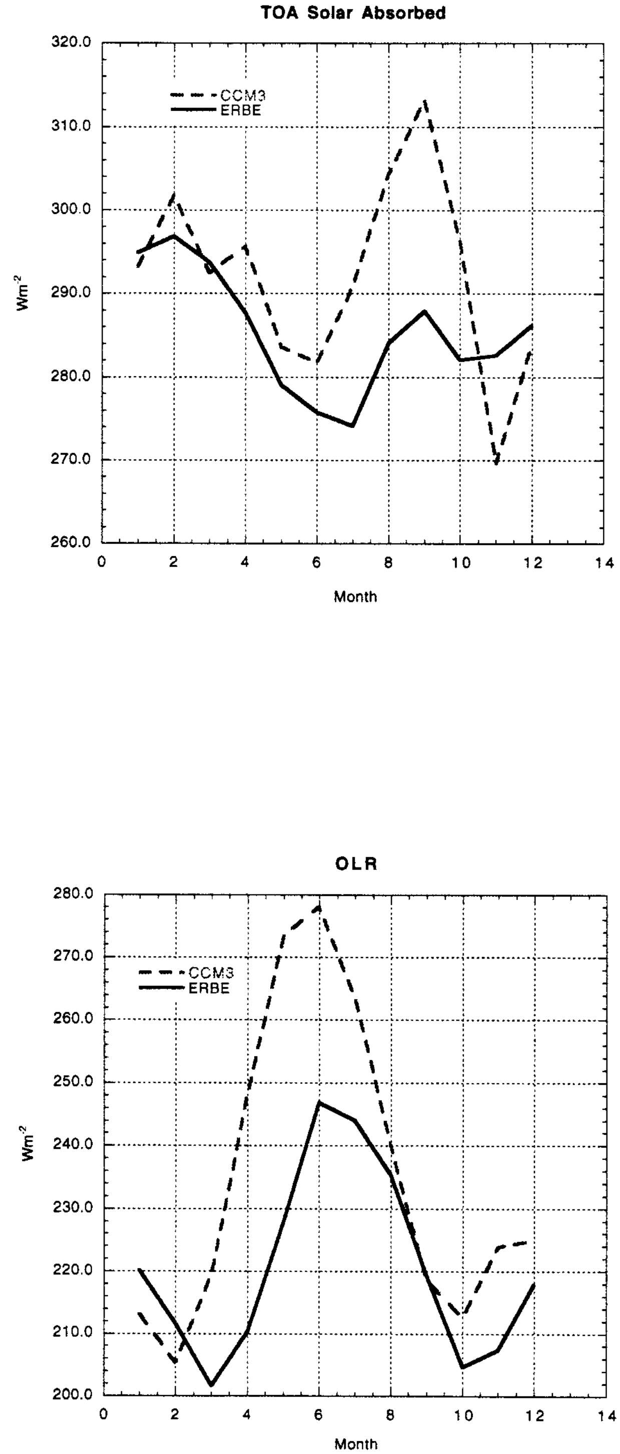

FIG. 33. Seasonal cycle for the Congo region of the (a) TOA shortwave absorbed flux and (b) outgoing longwave flux from CCM3 (– – –) and ERBE. Fluxes are in units of W m^{-2}.

degradation results from the new deep convection scheme, which shifted the vertical distribution of cloud cover to the upper-tropical troposphere. This shift in cloud cover (and associated shift in cloud optical properties) has led to the degradation in the slope. Research is currently under way to test new cloud microphysics schemes in the CCM3 in order to improve the relationship between δSWCF and δLWCF.

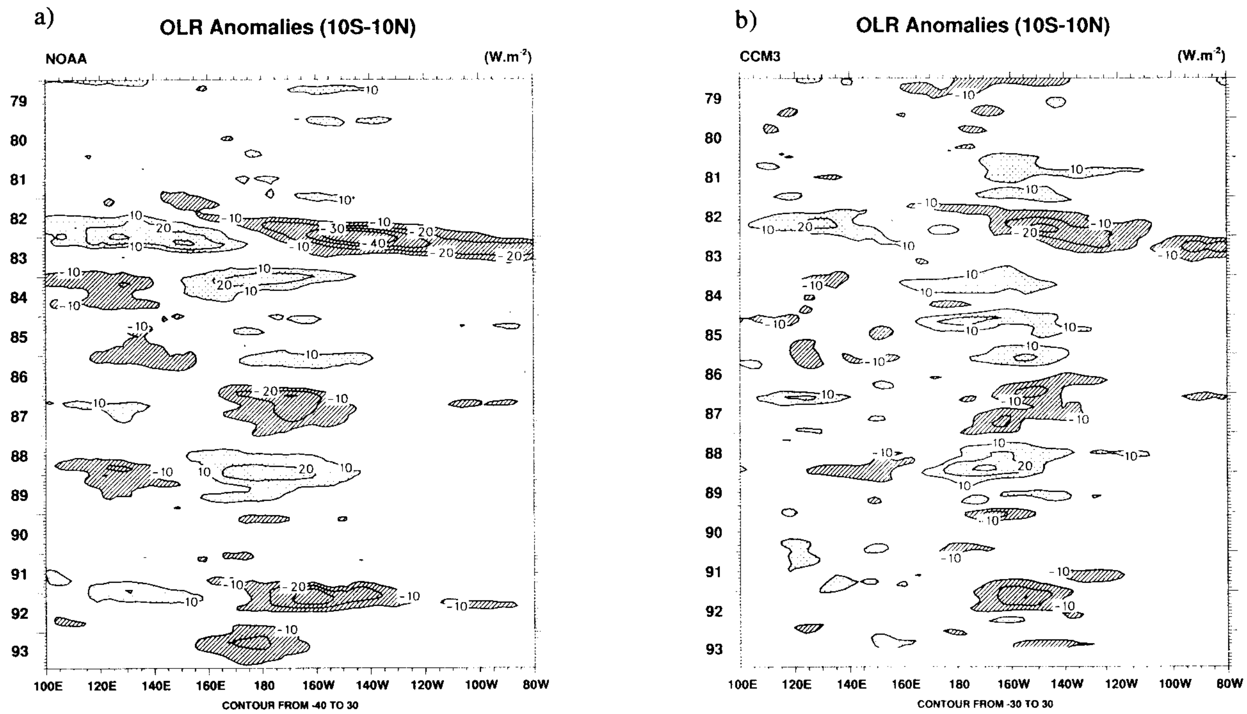

FIG. 34. Hovmöller of anomalies in OLR averaged across 10°S–10°N from (a) the NOAA satellite data and (b) the CCM3. Contour interval is 10 W m^{-2}.

7. Conclusions

The present study provides a detailed assessment of the energy budget of the latest version of the NCAR Community Climate Model (CCM3). We have compared both the top-of-atmosphere radiative flux of energy and surface energy fluxes with observational estimates of these fluxes. At the top of the atmosphere the agreement between the zonal-mean incoming and outgoing longwave radiation is in excellent ($<$10 W m^{-2}) agreement with ERBE data. Perhaps the largest bias is in the zonal-mean shortwave absorbed flux in the subtropics, where the model clouds are too bright compared to the ERBE data.

In terms of the geographic distribution there is in general good agreement between model and observations. The largest regional biases occur in the Tropics and areas of marine stratus in the subtropics. For example, the position of convection in the western Pacific is too far east compared to observations. In the eastern Pacific, the cloud forcing is too large compared to ERBE. The model simulation of clouds along the eastern boundaries of the Atlantic and Pacific Oceans, that is, marine stratus and stratocumulus, is deficient. This deficiency leads to large biases in the top-of-atmosphere and surface shortwave fluxes. The implication of this bias to the simulation of SSTs in the coupled model is discussed by Boville and Gent (1998).

At the surface, there is very good agreement over oceans between the CCM3 latent heat fluxes and those determined by Large et al. (1997). The largest bias at the surface over oceans is in the net shortwave flux reaching the surface. The Large et al. data indicate significantly ($\sim$25–35 W m^{-2}) less shortwave flux reaching the ocean surface compared to CCM3. Given the much smaller biases in shortwave absorbed flux at the top of the atmosphere, the most probable explanation is that the CCM clouds do not absorb sufficient shortwave radiation. This is a topic of active research at present (e.g., Ramanathan and Vogelmann 1997), and climate models must await the determination of the reason(s) for this enhancement of cloud absorption before implementing a parameterization into climate models.

The seasonal cycle of the CCM3 energy fluxes, both top of atmosphere and surface, for a number of regions is in good agreement with observations, especially over the oceans. Over midlatitude land, there is a bias in the models ability to represent the correct cloud distribution for summertime storm systems. In the Tropics, the differences over land are larger in both phase and magnitude.

The response of the top-of-atmosphere OLR to anomalies in tropical SSTs is simulated quite well in CCM3 compared to the observations from the NOAA satellites. This indicates that the shift in upper-tropospheric cloud associated with shifts in convective activity is realistically represented by the model. A deficiency in the response of the top-of-atmosphere energy budget to anomalies in SST is evident in the slope relationship between

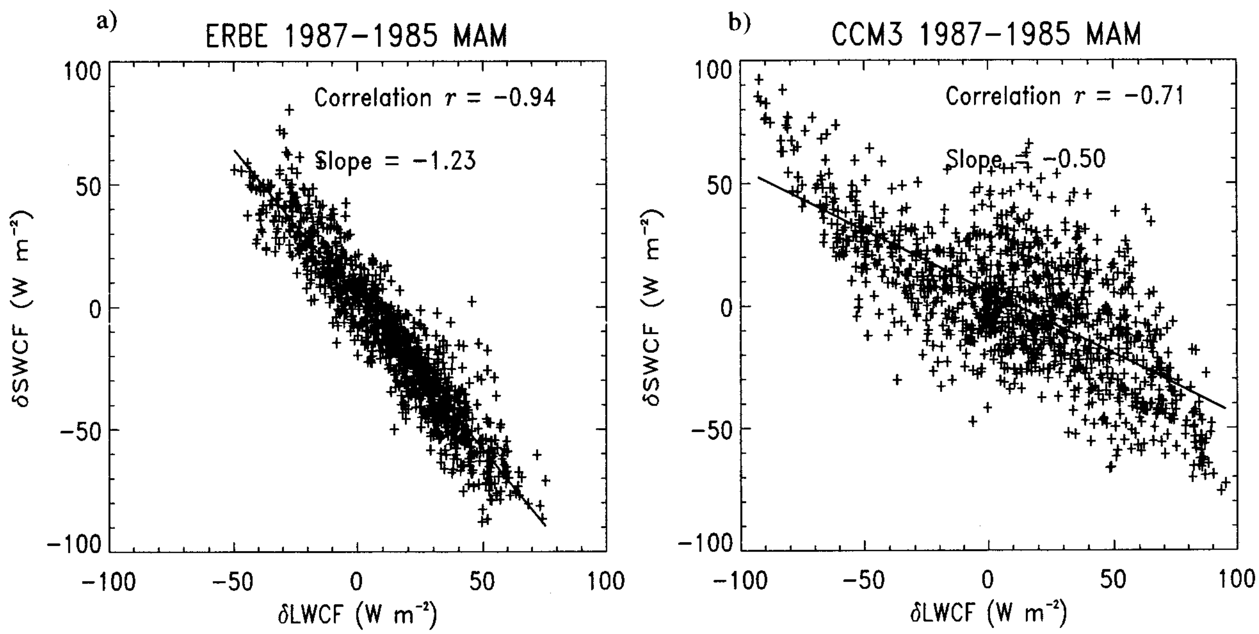

FIG. 35. Correlation between δSWCF and δLWCF (W m^{-2}) for the equatorial Pacific region from (a) ERBE data and (b) the CCM3. Delta is for the difference between March–May (MAM) 1987 and MAM 1985.

changes in SWCF correlated against changes in LWCF. The response of the SWCF to anomalies in SST is far too weak. This could be related to deficiencies in the cloud microphysics and/or shortwave optical properties of upper-tropospheric cloud. Improvements in this slope relationship are currently an active area of research by members of the NCAR Climate Modeling Section.

Overall the simulated energy budget of CCM3 at both the top of atmosphere and surface is in very good agreement with observations. A measure of success in simulating the surface energy budget is the good agreement between the implied ocean heat transport from the CCM3 compared with the explicitly simulated ocean heat transport from uncoupled ocean model. Opportunities for additional improvement are related to better parameterizations for convectively generated upper-tropospheric cloud and marine stratus clouds. There is also a need to incorporate realistic geographic variation and varying type of tropospheric aerosols.

Acknowledgments. We wish to thank Dr. C. S. Zender and Dr. W. D. Collins for their helpful comments. This work was supported in part by the DOE Atmospheric Radiation Measurements Program Grant DE-FG05-93ER61376.

REFERENCES

Andreae, M. O., 1995: Climatic effects of changing atmospheric aerosol levels. *World Survey of Climatology,* Vol. 16, *Future Climates of the World,* A. Henderson-Sellers, Ed., Elsevier, 341–392.

Bishop, J. K. B., and W. B. Rossow, 1991: Spatial and temporal variability of global surface solar irradiance. *J. Geophys. Res.,* **96,** 16 839–16 858.

Bonan, G., 1998: The land surface climatology of the NCAR Land Surface Model (LSM 1.0) coupled to the NCAR Community Climate Model (CCM3). *J. Climate,* **11,** 1307–1326.

Boville, B. A., and P. R. Gent, 1998: The NCAR Climate System Model, version 1. *J. Climate,* **11,** 1115–1130.

——, and J. Hurrell, 1998: A comparison of the atmospheric circulations simulated by the CCM3 and CSM1. *J. Climate,* **11,** 1327–1341.

Briegleb, B. P., 1992: Delta-Eddington approximation for solar radiation in the NCAR community climate model. *J. Geophys. Res.,* **97,** 7603–7612.

Chen, M., R. D. Cess, and M.-H. Zhang, 1995: Effects of longwave cloud radiative forcing anomalies on the atmospheric response to equatorial Pacific sea surface temperature anomalies. *J. Geophys. Res.,* **100,** 13 791–13 810.

Collins, W. D., J. Wang, J. T. Kiehl, G. J. Zhang, D. I. Cooper, and W. E. Eichinger, 1997: Comparison of tropical ocean–atmosphere fluxes with the NCAR Community Climate Model CCM3. *J. Climate,* **10,** 3047–3058.

Ebert, E. E., and J. A. Curry, 1992: A parameterization of ice cloud optical properties for climate models. *J. Geophys. Res.,* **97,** 3831–3836.

Gent, P. R., F. O. Bryan, G. Danabasaoglu, S. C. Doney, W. R. Holland, W. G. Large, and J. C. McWilliams, 1998: The NCAR Climate System Model global ocean component. *J. Climate,* **11,** 1287–1306.

Gleckler, P. J., and B. C. Weare, 1995: Uncertainties in global ocean surface heat flux climatologies derived from ship observations. PCMDI Rep. 26, 40 pp. [Available from OSTI, P.O. Box 62, Oak Ridge, TN 37831.]

——, and Coauthors, 1995: Cloud-radiative effects on implied oceanic energy transports as simulated by atmospheric general circulation models. *Geophys. Res. Lett.,* **22,** 791–794.

Hack, J. J., 1998: Sensitivity of the simulated climate to a diagnostic formulation for cloud liquid water. *J. Climate,* in press.

——, J. T. Kiehl, and J. W. Hurrell, 1998: The hydrologic and thermodynamic characteristics of the NCAR CCM3. *J. Climate,* **11,** 1179–1206.

Harrison, E. F., P. Minnis, B. R. Barkstrom, V. Ramanathan, R. D. Cess, and G. G. Gibson, 1990: Seasonal variation of cloud radiative forcing derived from the Earth Radiation Budget Experiment. *J. Geophys. Res.,* **95,** 18 687–18 703.

Hurrell, J. W., and G. G. Campbell, 1992: Monthly mean global satellite data sets available in CCM history tape format. NCAR Tech. Note NCAR/TN-371+STR, 94 pp. [Available from NCAR, Boulder, CO 80307.]

——, J. J. Hack, B. A. Boville, D. L. Williamson, and J. T. Kiehl, 1998: The dynamical simulation of the NCAR Community Climate Model version 3 (CCM3). *J. Climate,* **11,** 1207–1236.

Kalnay, E., and Coauthors, 1996: The NCEP/NCAR 40-year reanalysis project. *Bull. Amer. Meteor. Soc.,* **77,** 437–471.

Kerr, R. A., 1995: Climate modeling's fudge factor comes under fire. *Science,* **265,** 1528.

Kiehl, J. T., 1994a: Sensitivity of a GCM climate simulation to differences in continental versus maritime cloud drop size. *J. Geophys. Res.,* **99,** 23 107–23 115.

——, 1994b: On the observed near cancellation between longwave and shortwave cloud forcing in tropical regions. *J. Climate,* **7,** 559–565.

——, 1998: Simulation of the tropical Pacific warm pool with the NCAR Climate System Model. *J. Climate,* **11,** 1342–1355.

——, and V. Ramanathan, 1990: Comparison of cloud forcing derived from the Earth Radiation Budget Experiment with that simulated by the NCAR community climate model. *J. Geophys. Res.,* **95,** 11 679–11 698.

——, and B. P. Briegleb, 1992: Comparison of the observed and calculated clear sky greenhouse effect: Implications for climate studies. *J. Geophys. Res.,* **97,** 10 037–10 049.

——, and K. E. Trenberth, 1997: Earth's annual global mean energy budget. *Bull. Amer. Meteor. Soc.,* **78,** 197–208.

——, J. J. Hack, and B. P. Briegleb, 1994: The simulated earth radiation budget of the National Center for Atmospheric Research community climate model CCM2 and comparisons with the Earth Radiation Budget Experiment (ERBE). *J. Geophys. Res.,* **99,** 20 815–20 827.

——, ——, M. H. Zhang, and R. D. Cess, 1995: Sensitivity of a GCM climate to enhanced shortwave cloud absorption. *J. Climate,* **8,** 2200–2212.

——, ——, G. B. Bonan, B. B. Boville, B. P. Briegleb, D. L. Williamson, and P. J. Rasch, 1996: Description of the NCAR Community Climate Model (CCM3). NCAR Tech. Note NCAR/TN-420+STR, 152 pp. [Available from NCAR, Boulder, CO 80307.]

——, ——, ——, ——, D. Williamson, and P. J. Rasch, 1998: The National Center for Atmospheric Research Community Climate Model: CCM3. *J. Climate,* **11,** 1131–1149.

Klein, S. A., and D. L. Hartmann, 1993: The seasonal cycle of low stratiform clouds. *J. Climate,* **6,** 1587–1606.

Large, W. G., G. Danabasoglu, S. C. Doney, and J. C. McWilliams, 1997: Sensitivity to surface forcing and boundary layer mixing in a global ocean model: Annual-mean climatology. *J. Phys. Oceanogr.,* **27,** 2418–2447.

Mokhov, I. I., and M. E. Schlesinger, 1994: Analysis of global cloudiness 2. Comparison of ground-based and satellite-based cloud climatologies. *J. Geophys. Res.,* **99,** 17 045–17 065.

Oberhuber, J. M., 1988: An atlas based on the ''COADS'' data set: The budgets of heat, buoyancy and turbulent kinetic energy at the surface of the global ocean. Max-Planck Institute for Meteorology Rep. 15, 199 pp. [Available from Max-Planck-Institut für Meteorologie, Bundesstr. 55, D-20146 Hamburg, Germany.]

Ohmura, A., and H. Gilgen, 1993: Re-evaluation of the global energy balance. *Interactions between Global Climate Subsystems: The Legacy of Hann, Geophys. Monogr.,* No. 75, Int. Union Geodesy and Geophys., 93–110.

Porter, J. N., and A. D. Clarke, 1994: A new marine model and the optical response from satellite. *Proc. Eighth Conf. on Atmospheric Radiation,* Nashville, TN, Amer. Meteor. Soc., 473–474.

Ramanathan, V., and W. Collins, 1991: Thermodynamic regulation of ocean warming by cirrus clouds deduced from observations of the 1987 El Niño. *Nature,* **351,** 27–32.

——, and A. M. Vogelmann, 1997: Greenhouse effect, atmospheric solar absorption and the earth's radiation budget: From the Arrenhus-Langley era to the 1990s. *Ambio,* **26,** 38–46.

——, R. D. Cess, E. F. Harrison, P. Minnis, B. R. Barkstrom, E. Ahmad, and D. L. Hartmann, 1989: Cloud radiative forcing and climate: Results from the Earth Radiation Budget Experiment. *Science,* **243,** 57–63.

——, B. Subasilar, G. J. Zhang, W. Conant, R. D. Cess, J. T. Kiehl, H. Grassl, and L. Shi, 1995: Warm pool heat budegt and shortwave cloud forcing: A missing physics? *Science,* **267,** 499–503.

Rossow, W. B., and R. A. Schiffer, 1991: ISCCP cloud data products. *Bull. Amer. Meteor. Soc.,* **72,** 2–20.

——, and Y.-C. Zhang, 1995: Calculation of surface and top of atmosphere radiative fluxes from physical quantities based in ISCCP data sets. Part II: Validation and first results. *J. Geophys. Res.,* **100,** 1167–1197.

Trenberth, K. E., and A. Solomon, 1994: The global heat balance: Heat transports in the atmosphere and ocean. *Climate Dyn.,* **10,** 107–134.

Villevalde, Y. V., A. V. Smirnov, N. T. O'Neill, S. P. Smyshlyaev, and V. V. Yakovlev, 1994: Measurement of aerosol optical depth in the Pacific Ocean and the North Atlantic. *J. Geophys. Res.,* **99,** 20 983–20 988.

Warren, S. G., C. J. Hahn, J. London, R. M. Chervin, and R. L. Jenne, 1988: Global distribution of total cloud cover and cloud type amounts over ocean. NCAR Tech. Note TN-317+STR, 107 pp. [Available from NCAR, Boulder, CO 80307.]

Weaver, C. P., and V. Ramanathan, 1996: The link between summertime cloud radiative forcing and extratropical cyclones in the North Pacific. *J. Climate,* **9,** 2093–2109.

Zhang, G. J., J. T. Kiehl, and P. J. Rasch, 1998: Response of climate simulation to a new convective parameterization in the National Center for Atmospheric Research Community Climate Model (CCM3). *J. Climate,* in press.

Zhang, M. H., W. Y. Lin, and J. T. Kiehl, 1998: Bias of atmospheric shortwave absorption in the NCAR CCM: Comparison with monthly ERBE/GEBA measurements. *J. Geophys. Res.,* in press.